Hydrol. Earth Syst. Sci. Discuss., 12, 12433–12482, 2015
www.hydrol-earth-syst-sci-discuss.net/12/12433/2015/
doi:10.5194/hessd-12-12433-2015

Hydrology and Earth System Sciences
Open Access
Discussions

Assessing land–ocean connectivity via Submarine Groundwater Discharge (SGD) in the Ria Formosa Lagoon (Portugal): combining radon measurements and stable isotope hydrology

C. Rocha[1], C. Veiga-Pires[1,2], J. Scholten[3], K. Knoeller[4], D. R. Gröcke[5], L. Carvalho[1,2], J. Anibal[1,2], and J. Wilson[1]

[1]Biogeochemistry Research Group, Geography Department, School of Natural Sciences, Trinity College Dublin, Dublin 2, Ireland
[2]CIMA-Marine and Environmental Research Center, Universidade do Algarve, Faro, Portugal
[3]Institute of Geosciences, University of Kiel, Kiel, Germany
[4]UFZ – Helmholtz Centre for Environmental Research Leipzig/Halle, Leipzig, Germany
[5]Department of Earth Sciences, Durham University, South Road, Durham, County Durham, DH1 3LE, UK

Received: 14 September 2015 – Accepted: 19 October 2015 – Published: 27 November 2015

Correspondence to: C. Rocha (rochac@tcd.ie)

Published by Copernicus Publications on behalf of the European Geosciences Union.

Abstract

Natural radioactive tracer-based assessments of basin-scale Submarine Groundwater Discharge (SGD) are well developed, but because of the different modes in which SGD takes place and the wide range of spatial and temporal scales under which the flow and discharge mechanisms involved occur, quantifying SGD while discriminating its source functions remains a major challenge. Yet, correctly identifying both the fluid source and composition is critical: when multiple sources of the tracer of interest are present, failure to adequately discriminate between them will lead to inaccurate attribution and the resulting uncertainties will affect the reliability of SGD solute loading estimates. This lack of reliability then extends to the closure of local biogeochemical budgets, confusing measures aiming to mitigate pollution.

Here, we report a multi-tracer study to identify the sources of SGD, distinguish its component parts and elucidate the mechanisms of their dispersion throughout the Ria Formosa – a seasonally hypersaline lagoon in Portugal. We combine radon budgets that determine the total SGD (meteoric + recirculated seawater) in the system with stable isotopes in water (^{2}H, ^{18}O), to specifically identify SGD source functions and characterize active hydrological pathways in the catchment. Using this approach, SGD in the Ria Formosa could be separated into a net water input and another involving no net water transfer, i.e. originating in seawater recirculation through permeable sediments. The former SGD mode is present occasionally on a multiannual timescale, while the latter is a permanent feature of the system. In the absence of meteoric SGD inputs, seawater recirculation through beach sediments occurs at a rate of $\sim 1.4 \times 10^{6}\,m^{3}\,day^{-1}$, implying the entire tidal-averaged volume of the lagoon is filtered through local sandy sediments within 100 days, or about 3.5 times a year, driving an estimated nitrogen (N) load of $\sim 350\,t\,N\,yr^{-1}$ into the system as NO_3^-. Land-borne SGD could add a further $\sim 61\,t\,N\,yr^{-1}$ to the lagoon. The former source is autochthonous, continuous and responsible for a large fraction (59 %) of the estimated total N inputs into the system

HESSD

12, 12433–12482, 2015

Assessing land–ocean connectivity via SGD in the Ria Formosa Lagoon

C. Rocha et al.

via non-point sources, while the latter is an occasional allochthonous source, so more difficult to predict, but capable of driving new production in the system.

1 Introduction

Freshwater inputs into the coastal zone are important pathways for the transfer of land-borne solutes and particulates into the sea. Even if channeled freshwater flows such as rivers are relatively well-gauged world wide, sub-surface sources are more difficult to quantify in coastal settings. This difficulty has hindered the understanding of current drivers of coastal ecosystem decline (Carpenter et al., 1998; Finkl and Krupa, 2003). Indeed, $\sim 6\,\%$ of the freshwater input into the sea, carrying an anticipated 52 % of the total dissolved salts crossing the land–ocean interface, is estimated to occur via SGD-Submarine Groundwater Discharge (Zektser and Loaiciga, 1993) but mass flows defining the contribution of SGD to coastal biogeochemical budgets are difficult to quantify in a systematic way (Burnett et al., 2001a).

While the classical hydrogeologist might see SGD as a unidirectional freshwater flux driven by continental recharge, to understand the contribution of groundwater/seawater interactions to marine biogeochemistry (Moore, 1996, 2006; Moore and Church, 1996; Church, 1996), a more abragent definition of SGD needs to encompass any flow of water across the sea floor, regardless of fluid composition or driving force (Burnett et al., 2003). This is because reactivity of solutes when meteoric and sea water mix and travel through porous media significantly alters the composition of the discharging water with respect to both original contributions (Moore, 1999, 2010). This definition of SGD is therefore distinct from the traditional perspective in hydrogeology in that it is not limited to fresh groundwater discharge but includes seawater recirculation through coastal sediments (Li et al., 1999) and seasonal repositioning of the salt/freshwater interface (Michael et al., 2005; Edmunds, 2003; Santos et al., 2009). All of these promote changes to the rates of transfer, mixing and chemical reaction at the subterranean estuary (Moore, 1999; Charette et al., 2005; Charette and Sholkovitz, 2006; Robinson

HESSD
12, 12433–12482, 2015

et al., 2007) altering the original chemical signatures in a non-uniform way at system scale (Slomp and van Cappellen, 2004; Spiteri et al., 2008).

Tracer-based assessments of basin-scale SGD are well developed (Burnett et al., 2001a, b, 2003, 2008), but because the flow and discharge mechanisms involved cover a wide range of spatial and temporal scales (Bratton, 2010; Santos et al., 2012), quantifying SGD while discriminating its source functions is still a challenge (e.g. Mulligan and Charette, 2006). Indeed, the most common approaches to estimate SGD are: (a) radioactive tracer studies specifically looking at radon (^{222}Rn, $T_{1/2}$ = 3.8 days) (Burnett et al., 2001a, b) and radium isotopes (Moore and Arnold, 1996); (b) direct measurement of discharge fluxes over small areas (Lee, 1977); and (c) modeling. Direct measurements offer limited spatial coverage and are labor intensive (e.g. Leote et al., 2008), making reliable flux estimates at the system scale difficult. Modeling approaches depend on the water and/or salt budgets, hydrograph separation techniques, or descriptions of interfacial flow dynamics based on Darcy's law. Generally however, they incorporate assumptions of a steady state inventory and homogeneity of hydraulic conductivity over large scale-lengths and fail to include seawater recirculation. In addition, there is often a mismatch between spatial and/or temporal scale of the model outputs and those necessary to close coastal biogeochemical budgets (Prieto and Destouni, 2010).

Radioactive tracer studies produce spatially integrated estimates of flux (Cable et al., 1996; Moore, 1996), while simultaneously dampening the effects of short-term variability (Burnett et al., 2001a). However, while radon budgets produce an estimate of "total" SGD, i.e. freshwater inputs + re-circulated seawater (Mulligan and Charette, 2006), radium budgets primarily assess the salty component of SGD given that radium is normally absent in groundwater but might be mobilized from sediment particles in case of saline water influence (Webster et al., 1995). Even so, the variety of ubiquitous temporally and spatially variable sediment-water exchange mechanisms that also act as sources of radon (Cable et al., 2004; Martin et al., 2004; Colbert et al., 2008a, b) and short-lived radium isotopes to surface waters (Webster et al., 1994; Hancock and Mur-

HESSD
12, 12433–12482, 2015

ray, 1996; Hancock et al., 2000; Colbert and Hammond, 2007, 2008; Gonneea et al., 2008) cannot be ignored. Correctly identifying both the fluid source and composition is thus an important task (Mulligan and Charette, 2006; Burnett et al.,2006). When multiple tracer sources of interest are present, failure to adequately discriminate between them will lead to inaccurate attribution and the resulting uncertainties will affect the reliability of SGD solute loading estimates.

Indeed, as noted by Beck et al. (2007), SGD-borne chemical load into coastal systems is usually predicted by combining measurements of source composition with SGD estimates. A well supported causal chain linking these two datasets is therefore a key requisite: while the final flow estimate depends on how accurate our recognition of the SGD source(s) function(s) is (are), the ability to track its (their) path within the system is required to evaluate the biogeochemical history of the source functions prior to their mixture into receiving waters. Not fulfilling this requisite therefore constitutes the major obstacle so far to progress beyond our ability to prognosticate upper boundary or "potential" SGD-related impact, and more importantly, confidently attribute causality. The current panorama of SGD research at the system scale therefore begs the question of which end-member to use when selecting a source solute concentration in attempts to quantify pollutant fluxes associated with SGD.

We contribute an answer to this conundrum in a multi-tracer study conducted in a seasonally hypersaline lagoon in southern Portugal. The occurrence of SGD comprising significant freshwater contributions was first detected in the Ria Formosa in 2006–2007 and subsequently described as a prominent source of nutrients into the system (Leote et al., 2008; Rocha et al., 2009; Ibánhez et al., 2011, 2013). However, given the unpredictable nature of freshwater availability in the region, coupled with a mixed-source (i.e. a variable mix of groundwater abstraction and surface water collected in reservoirs) management of public water supply to meet demand (Monteiro and Costa Manuel, 2004; Stigter and Monteiro, 2008), it is not yet clear whether meteoric groundwater would be a persistent feature of SGD into the system. The overarching aims of the study were therefore to identify the sources of SGD, distinguish its

HESSD
12, 12433–12482, 2015

component parts and elucidate the mechanisms of their dispersion throughout the Ria Formosa.

We accomplish this aim by combining two datasets: radon surveys are used to determine total SGD in the system while stable isotopes in water (^{2}H, ^{18}O) are used to specifically identify SGD source functions and characterize active hydrological pathways. Even though correlations between δ^{18}O and δ^2H are central to research into the effect of evaporation and mixing on surface waters (Gat et al., 1994; Gibson and Edwards, 2002) and contribute to the disentanglement of different water sources affecting catchments (Rodgers et al., 2005), they are rarely used in coastal system hydrology. This is because paired δ^{18}O–δ^2H data on coastal seawater are sparse (e.g. Rohling, 2007), even though stable isotope datasets might help constrain the origins of freshwater inputs into the ocean when coupled with salinity data (Munksgaard et al., 2012). Here we also bridge the disciplinary gap between marine chemists and hydrogeologists currently extant in SGD studies by using a combined approach merging techniques from both disciplines.

2 Study site

2.1 Geomorphology and hydrodynamics

Located in south Portugal (36°58′ N, 8°02′ W–37°03′ N, 7°32′ W), the Ria Formosa (Fig. 1) is a leaky (Kjerfve, 1986) lagoon system separated from the Atlantic by a multi-inlet barrier island cordon. The system covers a surface area of $\sim 111\,\mathrm{km}^2$ and has an average depth of 2 m. The tide is semi-diurnal with average ranges of 2.8 m for spring tides and 1.3 m for neap tides (Vila-Concejo et al., 2004; Pacheco et al., 2010). The maximum average tidal volume as estimated by the Navy Hydrographical Institute (IH, 1986) is $\sim 140 \times 10^6\,\mathrm{m}^3$. Lagoon water is exchanged with the Atlantic Ocean through six tidal inlets with an average tidal flux of $\sim 8 \times 10^6\,\mathrm{m}^3$ (Balouin et al., 2001). Estimates for the submerged area amount to $\sim 55\,\mathrm{km}^2$ at high spring tide and between 14

HESSD
12, 12433–12482, 2015

and 22 km^2 at low spring tide (IH, 1986). From west to east (Fig. 1), inlets (*Barra*, in Portuguese) are identified as Ancão, Faro-Olhão (*Barra Nova*), Armona (*Barra Velha*), and Fuzeta, Tavira and Lacem (the 3 latter inlets are to the east of the region depicted in Fig. 1). Barra Nova, Barra Velha and Ancão jointly capture ~ 90 % of the total tidal prism: 61, 23 and 8 % of the total flow during spring tides and 45, 40 and ~ 5 % during neap tides, respectively (Pacheco et al., 2010). With the exception of the Barra Nova all inlets are ebb dominated with residual circulation directed seaward (Dias and Sousa, 2009).

2.2 Hydrogeological setting

The regional climate is semi-arid, with average annual temperature of 17 °C and averages of 11 and 24 °C during winter and summer. The surrounding watershed covers 740 km^2 and receives effective precipitation of 152 mm yr^{-1} (Salles, 2001). This corresponds to a potential annual rainfall of ~ 1.2×10^6 m^3, very small compared to the tidal exchange flux – hence the high average salinity of 35 found throughout the year in the lagoon (Mudge et al., 2008). There are five minor rivers and fourteen streams discharging into the lagoon. Most are ephemeral and dry out during the summer, the exception being the River Gilão, which intermittently discharges almost directly into the Atlantic through the Tavira inlet at the eastern limits of the system.

Three aquifer systems (Fig. 1) border the Ria Formosa (Almeida et al., 2000). These are the Campina de Faro (M12), Chão de Cevada–Quinta João de Ourém (M11) and São João da Venda–Quelfes (M10). The main lithologies supporting these units are Plio–Quaternary, Miocene and Cretaceous formations, comprising respectively Pliocene sands and gravels, Quaternary dunes and alluvial deposits; sandy limestones of marine facies; and limestones and detritic limestones. The oldest formation dips to the south, and is found at depths in excess of 200 m near the city of Faro. It is overlain by the Miocene formation extending below the Ria Formosa into the Atlantic ocean. Sand dunes, sands and gravels of the Plio–Quaternary cover the Miocene and Creta-

HESSD
12, 12433–12482, 2015

ceous formations within the coastal area. The Campina de Faro (M12, Fig. 1, 86.4 km^2) comprises a superficial unconfined aquifer (Pleistocene deposits) with a maximum thickness of 30 m and an underlying Miocene confined multi-layered aquifer, which Engelen and van Beers (1986) suggest discharges directly into the Atlantic Ocean bypassing the lagoon. The two units are hydraulically connected. The Sao João da Venda-Quelfes aquifer (M10, Fig. 1, 113 km^2) includes a surface 75 m thick layer of Wealdian facies and an underlying Cretaceous layer of loamy limestone. It contacts with the M12 (Campina de Faro) aquifer and the M11 (Chão de Cevada–Quinta João de Ourém) to the south, and the main flow direction on the eastern side is towards the southeast. Groundwater flow is divergent toward the southeast and the southwest from a central point (Almeida et al., 2000).

In the 1980's nitrate contamination from inorganic fertilizers was detected in both Quaternary and Miocene sub-units of the Campina de Faro (M12) aquifer (Almeida and Silva, 1987). Average concentrations where 8.3 mmol L^{-1} with some samples containing in excess of 28.6 mmol L^{-1}. More recently, Lobo-Ferreira et al. (2007) calculated an average concentration of 2.1 mmol L^{-1} over the entire aquifer, an estimate that is consistent with the long-term (1995–2011) average ($n = 31$) of 1.87 ± 0.35 mmol L^{-1} nitrate concentration reported from public groundwater quality data (http://www.snirh.pt) in a monitoring borehole in Montenegro, close the boundary with the Ria. During 2006–2007, nitrate and ammonium concentrations of up to 187 and 40 µmol L^{-1} respectively were measured in SGD collected by seepage meters deployed at the littoral zone of the barrier islands. The upper bound mean nitrate concentration in the freshwater component of SGD was estimated at ~ 0.4 mmol L^{-1} (Leote et al., 2008).

HESSD
12, 12433–12482, 2015

3 Methods

3.1 Radon measurements

3.1.1 Lagoon radon inventory during ebb and flood

Water radon (^{222}Rn) content was measured continuously in-situ using two electronic Durridge RAD-7 radon-in-air monitors deployed in tandem on a moving rubber boat during winter (December 2009) and spring (May 2010). Each monitor was coupled to an air–water equilibrator (Durridge RAD-Aqua Accessory) via its own air loop. Non-cavitating centrifugal pumps were used to flush water from ~ 50 cm below the water surface directly into the equilibrators, at a flow rate of 1.8–2.5 L min^{-1}. HOBO™ temperature sensors and a CTD diver (Schlumberger™) continuously recorded the temperature in the mixing chambers and the salinity and temperature of the water being pumped. Counting interval was set at 20 min on each RAD-7 monitor, with the two machines staggered by a 10 min period, allowing for simultaneous replication of 20 min integration periods over the route and increased temporal resolution. Full equilibration between the air within the air-loop and the pumped seawater was achieved before surveys started. Sampling began near low tide and continued without interval for 24 h. The survey path, recorded with an on-board GPS unit, and the timing were designed to cover the main navigable sectors of the whole lagoon at different tidal stages (ebb and flood) within the course of two complete tidal cycles. In-water radon activity was calculated from the temperature and salinity dependant gas/water equilibrium (Schubert et al., 2012). Radon activities obtained this way were then corrected by the local ^{226}Ra supported activity, to obtain excess (i.e. unsupported) radon activities. For mass balance purposes, the excess radon inventories were calculated by multiplying the unsupported radon activity from the continuous measurements by the local bathymetric depth, and then normalized to mean tidal height (Burnett and Dulaiova, 2003).

3.1.2 Tidal variability of radon activity at fixed locations

Time series of radon activity were obtained synchronously at two fixed locations within the Faro channel (Fig. 1), during June 2010. The locations were chosen in order to gain insight into the exchange of radon between the lagoon and the adjacent coastal zone through the Barra Nova (Fig. 1) and between the inner reaches of the lagoon and the latter via the Faro channel (Quatro-Águas, Fig. 1). Radon activity was measured as described previously, with the added deployment of a CTD diver (Schlumberger™) recording depth, salinity and temperature at the bottom of the channel. The Barra Nova tidal cycle data was then used to calculate the net exchange of radon with the adjacent coastal zone through the main inlet, assuming a vertically well-mixed water column. Exchange of radon through the inlet cross section driven by oscillating tidal flow was determined by first calculating the instantaneous directional flux, $F_{\text{Rn}}(\Delta t)$, where Δt is the counting interval, $A_{\text{Rn}}(\Delta t)$ the activity of radon integrated across the counting interval and $\mathrm{d}h/\mathrm{d}t$ the change in tidal height (r.m.s.l.) occurring over that interval:

$$F_{\text{Rn}}(\Delta t) = \left(\frac{\mathrm{d}h}{\mathrm{d}t}\right) \times A_{\text{Rn}}(\Delta t). \tag{1}$$

The total radon flux was obtained for both the flood and ebb periods by integrating the instantaneous directional fluxes calculated for each counting period (Eq. 1) over time. Radon outflow (when fluxes were negative) and inflow (when positive) are hence obtained for each complete semi-tidal period. Difference between successive outflow and inflow periods gives us the net transfer across the channel during a complete tidal cycle. Data for a minimum of three successive complete tidal cycles, giving three different values for net transfer, were used, and the exchange values determined for each cycle were then averaged to obtain the net exchange flux along the channel at each sampling site.

HESSD
12, 12433–12482, 2015

3.1.3 Complementary radon measurements

Measurements of air temperature, wind speed and atmospheric radon activities were taken on land, while the lagoon radon survey progressed. Atmospheric evasion losses (radon degassing flux) were calculated as described in Burnett and Dulaiova (2003), using the equations given in Macintyre et al. (1995) and Turner et al. (1996). Sediment-water diffusive fluxes of radon were measured as described in Corbett et al. (1998) in samples (n = 16) collected throughout the lagoon.

3.1.4 SGD flux estimates based on Rn mass balances

Lagoon Radon budget under steady state assumptions

The advective flux of radon associated with SGD is determined by the closure of a radon budget incorporating all known sources and sinks of radon in the system (Burnett and Dulaiova, 2003). Mass conservation accounting for the change in inventory of radon was expressed as:

$$\frac{\mathrm{d}I_{\mathrm{Rn}}}{\mathrm{d}t} = \mathrm{Rn_{diff}} - \mathrm{Rn_{dg}} - \mathrm{Rn_{dy}} + (\mathrm{Rn_{imp}} - \mathrm{Rn_{exp}}) + \mathrm{Rn_{adv}} \tag{2}$$

where I_{Rn} is the radon inventory measured within the Ria Formosa, t the time, $\mathrm{Rn_{diff}}$ the Radon flux across the sediment water interface by diffusion, $\mathrm{Rn_{dg}}$ the radon degassing flux, i.e. atmospheric evasion, $\mathrm{Rn_{dy}}$ the radon decay flux in the lagoon (i.e. the internal sink), $\mathrm{Rn_{exp}}$ and $\mathrm{Rn_{imp}}$ the exchange fluxes across inlets, seaward (export) and landward (import), respectively, and $\mathrm{Rn_{adv}}$ the advective Radon flux putatively associated with SGD. Usually, an additional term accounting for the radon influx via river flow is added if the water and particulate flux associated with river discharge is significant. However, the only perennial river in the Ria Formosa is the Gilão, located in the eastern limit of the lagoon. Salinity measured at the estuary mouth was 29.6 (Table S1 in the Supplement), which in combination with its location implied very low if any inputs of

HESSD
12, 12433–12482, 2015

freshwater carrying radon into the system so we neglected the term. Assuming steady state of all sinks and sources over the lifetime of radon in the system, then:

$$\frac{dI_{\mathrm{Rn}}}{dt} = 0, (\mathrm{Rn_{imp}} - \mathrm{Rn_{exp}}) = \mathrm{Rn_{net}} \Rightarrow \mathrm{Rn_{adv}} = \mathrm{Rn_{diff}} - \mathrm{Rn_{dg}} - \mathrm{Rn_{dy}} + \mathrm{Rn_{net}} \quad (3)$$

where $\mathrm{Rn_{net}}$ is the residual Radon exchange flux with the ocean.

Mass balance of radon during ebb and flood

Inventories of radon in the lagoon were determined during ebb and flood. Taking the tide as a travelling wave, the change in inventory of radon as the tide floods and ebbs has to be balanced by all known radon fluxes occurring within the traversed system during the travel period. If we then take the mean tide level (MTL) as a reference, it follows that the $\mathrm{Rn_{adv}}$ term may be calculated for different periods: the period at which the tidal height in the lagoon is below MTL ($\mathrm{Rn_{adv}}(T < \mathrm{MTL})$), i.e. the trough of the tidal wave or low tide, and the one when it is above MTL ($\mathrm{Rn_{adv}}(T > \mathrm{MTL})$), corresponding to the peak of the wave, or high tide. Assuming constant mean amplitude for the tidal wave the corresponding mass conservation equations may be written as follows:

$$\mathrm{Rn_{adv}}(T < \mathrm{MTL}) = \frac{I_{\mathrm{f}} - I_{\mathrm{e}}}{\Delta t} - (\mathrm{Rn_{net}} + \mathrm{Rn_{diff}} - \mathrm{Rn_{dg}} - \mathrm{Rn_{dy}}) \quad (4a)$$

$$\mathrm{Rn_{adv}}(T > \mathrm{MTL}) = \frac{I_{\mathrm{e}} - I_{\mathrm{f}}}{\Delta t} - (\mathrm{Rn_{net}} + \mathrm{Rn_{diff}} - \mathrm{Rn_{dg}} - \mathrm{Rn_{dy}}) \quad (4b)$$

where I_{f} and I_{e} are the flood and ebb inventories of radon in the lagoon, Δt the period of the wave (~ 0.5 day) and $\mathrm{Rn_{adv}}(T < \mathrm{MTL})$ and $\mathrm{Rn_{adv}}(T > \mathrm{MTL})$ the radon advective fluxes associated with each semi-period (trough and peak stages, respectively). The corresponding continuity equation, describing the net advective flux of radon on a daily basis (note that for semi-diurnal tidal periodicity we assume 1 day $\sim$ 2 tidal periods), is then:

$$\frac{\mathrm{Rn_{adv}}}{2\Delta t} = \frac{\mathrm{Rn_{adv}}(T < \mathrm{MTL})}{2} + \frac{\mathrm{Rn_{adv}}(T > \mathrm{MTL})}{2}. \quad (4c)$$

HESSD
12, 12433–12482, 2015

3.2 Stable isotope hydrology

Samples for stable isotope analysis of water were collected in triplicate from all possible water sources to the lagoon on various occasions between 2007 and 2013 (Table S1). These samples include: marine end-member; groundwater from local aquifer units (M10, M12, unconfined aquifer lenses in the Barrier island) taken from boreholes and wells (Fig. 1); precipitation, taken at the city of Faro; beach porewater, at various depths in the sediment (2 to 7 m below r.m.s.l) via a cross-shore array of nested, multi-level sampling piezometers installed in the inner margin of the outer dune cordon. Porewater was also extracted in 2007 from 50 cm below the sediment–water interface at various locations along the same dune cordon; Surface water reservoirs near Quinta do Lago used for irrigation in 2007; settling lagoons in the wastewater treatment plant near the city of Faro (WWTP) in 2007; the river Gilão, and finally surface water from the lagoon itself, taken at both high and low tide in 2009 and during flood tide (western sector, Stations 1–5 and 1B–5B) in 2007.

Quasi-synoptic distributions of $\delta^{18}O$ and $\delta^{2}H$ in water at different tidal stages were obtained for the lagoon in the winter of 2009. For this purpose, we divided the lagoon into two sectors, comprising western and eastern areas, with the separation line lying between the city of Faro and the Barra Nova. High powered boats were deployed, one from the city of Olhão, on the 5 December 2009 and one from the city of Faro, on the 2 December 2009 (Fig. 1). The boats followed the tide outflow (or inflow) while covering all the pre-defined sampling points (Fig. 1). Each region of the lagoon was covered at each tidal stage in no more than two hours around slack tide. Coastal seawater adjacent to the Ria Formosa was sampled two nautical miles (~ 3.8 km) offshore from the town of Quarteira to the west and from the Barra Velha (Armona inlet, Fig. 1, reference J).

Water was directly filtered through Rhizon SMS™ membranes into sterile glass Vaccutainer™ vials in the field. Subsequently, the cap area including the rubber septum was sealed with a layer of hot glue encased in Parafilm™. The vials were kept

HESSD
12, 12433–12482, 2015

preserved at 4 °C until analysis could occur (typically within six months from the date of collection). Samples were sent for standard analysis of $\delta^{18}O$ and $\delta^{2}H$ to GEOTOP Canada (Micromass IsoprimeTM dual inlet coupled to an Aquaprep TM system), Durham University (LGR – liquid water isotope analyser, DT100) and at UFZ's stable isotope laboratory facilities in Halle, Germany (Laser cavity ring-down spectroscopy (Laser CRDS) Picarro water isotope analyzer L-1120i). Following standard reporting procedures (Craig, 1961a), delta values (δ) are reported as deviations in permil (‰) from the Vienna Standard Mean Ocean Water (V-SMOW), such that $\delta_{\text{sample}} = 1000((R_{\text{sample}}/R_{\text{V-SMOW}}) - 1)$, where R is the relevant isotopic ratio (i.e. either $^{2}H/^{1}H$ or $^{18}O/^{16}O$). The mean analytical uncertainty is reported for each data point as ±1 SD (standard deviation) of the mean of n analysis results obtained for n replicate samples in ‰ for $\delta^{18}O$ and for $\delta^{2}H$ (see Table S1). Each laboratory uses stringent protocols and reporting of stable isotope values using internationally calibrated standards; hence, reported stable isotopes values of water between the different labs used in this study are directly comparable.

4 Results

4.1 Radon

4.1.1 Spatial and temporal distribution

The activity ranges and spatial distribution of ^{222}Rn were similar in winter and spring. Because the weather was stormy during winter sampling, uncertainty associated with radon evasion fluxes and in-water radon activities affecting the overall lagoon inventory were much higher than in spring. Hence only the spring survey data is presented. Excess radon activities measured in water varied between 3.5 and 37 Bq m^{-3}, with a narrower range (5–25 Bq m^{-3}) measured during ebb. The highest activities within the western sector during this stage (> 25 Bq m^{-3}) were measured close to the city of

HESSD
12, 12433–12482, 2015

Faro and in the Ramalhete channel, and close to the city of Olhão (~ 20 Bq m^{-3}) in the eastern sector. Radon activities generally declined from the northwest to the southeast during ebb tide, with the lowest values (~ 5 Bq m^{-3}) found in the Olhão channel northeast of the Barra Nova. Conversely, the lowest activities during flood (~ 5 Bq m^{-3}) were measured close to the Ancão inlet and at the outer end of the Faro channel, suggesting radon-poor coastal water intrusion during flood tide. The mean radon activities throughout the lagoon were 19.3 ± 4.74 and 15.59 ± 4.54 Bq m^{-3} respectively during flood and ebb. Relative accumulation of radon occurred at specific locations in the lagoon (Fig. 2a and b). The highest local water column inventories (318 and 267 Bq m^{-2} during flood and ebb, respectively) were found in the Faro channel, covering stations 3 to A during ebb and 4 and 5 during flood. The eastern sector water column inventories where much higher during flood than during ebb. Given the non-random spatial distribution of radon, the median of each dataset was used to calculate whole-lagoon inventories. The MAD (median absolute deviation, Hampel, 1974) was then used to propagate uncertainty in the radon budget calculations (Table 1). Radon inventories (median ± MAD) were 54.2 ± 17.8 and 74.0 ± 17.6 Bq m^{-2} respectively during ebb and flood (Table 1).

4.1.2 Along-channel tidal radon fluxes

Radon activity at Quatro Águas and Barra Nova was strongly anti-correlated with water level. At Quatro Águas, radon activities varied between 0 and 40 Bq m^{-3} while at Barra Nova they varied between 1 and 31 Bq m^{-3}. Tidal variability at these two points was therefore consistent with the ranges in radon activity found during the lagoon survey. Time series of instantaneous Rn fluxes obtained as described by Eq. (1) are depicted for both locations in Fig. 3. The plots show consistency in the magnitude of upstream and downstream radon fluxes (grey area under the curves) through successive tidal cycles. The net daily tidal exchanges of radon through the Barra Nova and the Quatro Águas site (8.0±0.5 × 10^{4} and 9.9±2.0 × 10^{3} Bq day^{-1}, respectively) were both directed landward. This finding is consistent with the Barra Nova being a flood-dominated inlet (channeling ∼ 64 % of the flood and ∼ 59 % of the ebb prism of the Ria Formosa during spring tides: Dias and Sousa, 2009; Pacheco et al., 2010). To calculate the total residual exchange of radon between the Ria Formosa and the adjacent coastal area, we assumed the radon flux occurring at the other inlets to be proportional in equal measure to the individual residual tidal prisms. After adjustment to the lagoon surface area at MTL the net exchange was just $-9.3\,(\pm 1.6) \times 10^{-4}\,\mathrm{Bq\,m^{-2}\,day^{-1}}$ (Table 1), so small as to be well within the uncertainty of all other quantities in the mass balance, implying that the radon inventory within the lagoon is controlled by internal fluxes.

4.1.3 SGD estimates based on radon mass balance

Solving Eq. (3) for a radon inventory of $65.9 \pm 19.6\,\mathrm{Bq\,m^{-2}}$ (Table 1) gave a result for Rn_{adv} of $7.14 \pm 5.18\,\mathrm{Bq\,m^{-2}\,day^{-1}}$, which adjusted to the submerged area at mean tide level (Tett et al., 2003) gives an SGD derived radon flux of $4.14\,(\pm 3.00) \times 10^{8}\,\mathrm{Bq\,day^{-1}}$ for the entire lagoon. Alternatively, the advective radon fluxes calculated as per Eqs. (4a) and (4b) for low and high tide periods were respectively 46.8 ± 38.8 and $-32.5 \pm 27\,\mathrm{Bq\,m^{-2}\,day^{-1}}$. The positive and negative signs imply an advective flux of radon (Rn_{adv}) into the lagoon water column at low tide, while a net loss occurs during high tide. The resultant net Rn_{adv} (Eq. 4c) occurring during a full tidal period is $7.15 \pm 8.4\,\mathrm{Bq\,m^{-2}\,day^{-1}}$, statistically equivalent to the flux calculated via the assumption of steady state of the system over the lifetime of radon on a daily timescale, and yielding an equivalent SGD-derived radon flux of $4.14\,(\pm 4.87) \times 10^{8}\,\mathrm{Bq\,day^{-1}}$ for the entire lagoon.

HESSD
12, 12433–12482, 2015

4.2 Stable isotope hydrology

4.2.1 $\delta^{18}O$ vs. $\delta^{2}H$ relationships in the catchment

Water stable isotope compositions obtained during this study, as well as Global Network of Isotopes in Precipitation (GNIP) (IAEA/WMO, 2013) and other literature-sourced data (Carreira, 1991) are listed in Table S1. During the 2007 survey only unit M12 was sampled for fresh groundwater while during 2009–2011 both the M12 and M10 aquifer units were sampled. Nonetheless the compositional range of fresh groundwater samples was quite similar: the most depleted values reported had a $\delta^{18}O$ value of −5.09 ‰ (Pechão Gimno, M10) and a $\delta^{2}H$ value of −27.79 ‰ (Gambelas, M12) while the most enriched had a $\delta^{18}O$ value of −3.46 ‰ (Rio Seco, M12) and a $\delta^{2}H$ value of −21.45 ‰ (Zona industrial, M12). The compositional ranges of ~ 1.63 ‰ for $\delta^{18}O$ and ~ 6.34 ‰ for $\delta^{2}H$ for groundwater were much narrower than those found in GNIP records for the city of Faro (respectively ~ 8.43 and ~ 57.3 ‰). Nevertheless (Fig. 4a), the amount-weighed average isotope composition of precipitation inputs into the Ria Formosa catchment ($\delta^{18}O = -4.8$ ‰ and $\delta^{2}H = -27.13$ ‰) taken from the GNIP dataset (1978–2001) plots slightly above the Global Meteoric Water Line (GMWL, Clark and Fritz, 1997) and below the Western Mediterranean Meteoric Water Line (WMMWL, Celle-Jeanton et al., 2001). In conjunction with the average isotopic composition of groundwater in the catchment, that of seawater (Carreira, 1991) and adjacent coastal water, a precipitation-seawater mixing line (PP-SW Mix, Fig. 4) may be defined ($\delta^{2}H = 5.37 \times \delta^{18}O - 1.7$, $r^2 = 0.99$). The slope of this mixing line is similar to that found by Munksgaard et al. (2012) for the Great Barrier Reef (i.e. 5.66). Additional relationships framing the isotopic composition of the waters in the catchment in δ space include the Local Meteoric Water Line (LMWL), defined by Carreira et al. (2005) as $\delta^{2}H = (6.44 \pm 0.24) \times \delta^{18}O + (3.41 \pm 1.13)$ and the Eastern Mediterranean Meteoric Water Line (EMMWL, Gat and Carmi, 1970). This is introduced as an extreme boundary to the isotopic composition of precipitation in southern Portugal. Indeed, rain with high *d-excess* originating either from the eastern Mediterranean or

HESSD
12, 12433–12482, 2015

aligned with extreme precipitation events might fall in the region (see Fig. 4c), particularly during summer and/or autumn (e.g. Frot et al., 2007).

4.2.2 $\delta^{18}O$ and δ^2H in groundwater

In 2007, the stable isotope composition of groundwater in M12 reveals slight evaporative enrichment by comparison to the GMWL and LMWL, plotting along the precipitation seawater mixing line (Fig. 4b). The isotopic compositions of surface waters (WWTP settling lagoons and lagoon surface waters) and porewaters plotted between the LMWL and the PP-SW mixing line (Fig. 4b), suggesting their composition was controlled by the interplay between the mixture of sea and groundwater and evaporation–condensation cycles occurring along the hydrological travel path. In 2009–2011 however, the range of isotopic compositions of surface water samples (~ 2.87 ‰ for $\delta^{18}O$ and ~ 3.96 ‰ for δ^2H) was significantly different (see inset, Fig. 4c). Their composition then fell between the WMMWL and the PP-SW mixing line. Even though the number of samples taken in 2007 was lower than those taken later and tide-specific sampling was absent, comparison of samples taken in both years at high tide slack (Table S1; Stations 2, 3, 4, A and 3B) shows the isotopic composition of water in the Ramalhete and Faro channels was distinct – the observed difference in range cannot therefore be attributed to the sampling strategy.

Groundwaters across the catchment could be divided into three distinct groups: samples from Pechão Gimno, Pechão Serra and Pechão Zona industrial (Table S1), all from unit M10, plot above the GMWL and the LMWL, while samples taken from the unconfined aquifer wells in the outer barrier islands belonging to the unconfined M12 aquifer (i.e. Deserta, Table S1), plot distinctly below the PP-SW mixing line. In between, M12 samples plot along (Ramalhete) and below the PP-SW Mixing line (Costa, Chelote, Rio Seco). Samples from unit M10 plot along a local evaporation line (LEL) with slope ~ 4.5 while samples from unit M12, excluding the ones located within the Ria Formosa proper, plot along a LEL with slope ~ 4.1.

HESSD
12, 12433–12482, 2015

4.2.3 Isotopic composition of beach porewater

The pore water isotope compositions differed significantly between 2007 and 2009–2011. Beach groundwater was sampled during spring and neap tides from sediment depths ranging from 50 cm to 3.5 m below MTL across a beach profile from the upper to the lower intertidal during the latter period. $\delta^{18}O$ ranged from 0.96 to −0.20 ‰ and $\delta^{2}H$ from 2.5 to 8.5 ‰ and plotted close to the LMWL (Fig. 5a) along an evaporation line defined by $\delta^2H = (4.02 \pm 0.56) \times \delta^{18}O + (4.51 \pm 0.31)$, $n = 24$, $r^2 = 0.702$, not shown). The slope of this LEL is slightly lower than those of the groundwater LELs (4.1 for the M12 and 4.5 for the M10). The data fell into three distinct groups (Fig. 5a and b) according to the relative position of the sampling point within the beach section. The first group of samples (average $\delta^{18}O$ of 0.0 ± 0.13 ‰ and δ^2H of 3.5 ± 0.93 ‰, $n = 5$) corresponded to the unsaturated and intermediate zones (upper intertidal), while the second (average $\delta^{18}O$ of 0.4 ± 0.31 ‰ and δ^2H of 6.1 ± 0.47 ‰, $n = 10$) and third groups (average $\delta^{18}O$ of 0.7 ± 0.18 ‰ and δ^2H of 8.0 ± 0.37 ‰, $n = 9$) were isotopically heavier and included in that order pore water from the deeper (> 2 m below the surface) and shallower (< 1 m below the surface) areas of the beach section. The respective average pore water stable isotope compositions plotted close to the LMWL (Fig. 5a), showing enrichment in opposition to distance from the surface in the saturated zone and depletion in the unsaturated recharge zone, probably due to capillarity effects (Barnes and Allison, 1988). The dependence of *d-excess* (Dansgaard, 1964) on $\delta^{18}O$ (Fig. 5b) illustrates the deviation of porewater composition from Craig's (1961b) GMWL ($\delta^2H = 8 \times \delta^{18}O + 10$) along significantly linear slopes dependant on local evaporation conditions. Indeed, porewater *d-excess* from deeper within the beach plots along the line defined by $d = -6.7\,(\pm 0.27) \times \delta^{18}O + 5.57\,(\pm 0.13)$ ($n = 10$, $r^2 = 0.987$, $P < 0.0001$) while that from shallower areas plots along the line defined by $d = -7.1\,(\pm 0.69) \times \delta^{18}O + 7.28\,(\pm 0.52)$ ($n = 9$, $r^2 = 0.937$, $P < 0.0001$). These define slopes in δ space close to 1 and are consistent with the flow paths taken by beach groundwater between the seawater infiltration point at the higher beach face (higher *d-excess*) and the exfiltration point at

HESSD
12, 12433–12482, 2015

the seepage face (lower *d-excess*). For the intermediate group of samples, longer flow paths (larger *d-excess* range) and less evaporative enrichment (lower average $\delta^{18}O$) are consistent with tidal-forced circulation at larger depths within the beach face. Conversely, shorter flow paths (relatively narrow *d-excess* range) and more evaporative enrichment (higher average $\delta^{18}O$) characterize shallower circulation pathways.

Interannual variability was also significant. The range of ∼ 1.16 ‰ for $\delta^{18}O$ and ∼ 6.03 ‰ for $\delta^{2}H$ found in 2009–2011 was 50 and 36 %, respectively, of the 2007 range, in spite of a common sampling location. Furthermore, isotopic compositions for pore water collected in 2007 plotted in δ space clearly in between the LMWL and the PP-SW mixing line (Fig. 4b), while the 2010–2011 samples overlap the LMWL (Figs. 4c and 5a). This occurs in spite of fewer samples being taken in 2007 and their depth of 50 cm below the surface, in contrast with the wide range of sediment depths sampled during 2009–2011. Paired ranges of pore water salinity also differ, varying between 21 and 36 in 2007 and between 36 and 43 in 2009–2011. These results suggest different water source functions were present during each sampling period.

4.2.4 Tidal variability of surface water δ^{18}O and δ^{2}H

Tides have a significant effect on the range of isotopic composition of surface water within the lagoon (see Fig. 6). In both lagoon sectors, the isotopic compositional range of water was much wider at low tide (Fig. 6a) than at high tide (Fig. 6b) but this variability was more apparent in the western sector. During low tide there $\delta^{2}H$ ranged from 5.3 ‰ (Station 2B) to 7.9 ‰ (Station 2) and $\delta^{18}O$ from −0.82 ‰ (Station 2B) to 2.05 ‰ (Station 3). By contrast, $\delta^{2}H$ ranged from 5.1 ‰ at Station 3B to 7.3 ‰ at 4B, while $\delta^{18}O$ varied from −0.16 ‰ (Station 4) to 0.86 ‰ (Stations 1B and 2B). The water mass at Station 2B was most depleted in ^{18}O during low tide (Fig. 6a) and the most enriched in ^{18}O during high tide (Fig. 6b) but remains at the lower end of the $\delta^{2}H$ range covered by all collected samples during both tidal stages. Aspects of tide-induced circulation are also revealed when the western and eastern sectors are compared for identical tidal stages (Fig. 6a and b). During low tide (Fig. 6a), the isotope compositions of water collected at the Ramalhete channel and the associated Ancão basin (Stations 1B to 5B, Fig. 1) plot to the left of the LMWL, with the most isotopically depleted water found in Station 2B and the most enriched found at Station 1B. Conversely, water samples collected in the Faro channel (Stations 1 to 5) plot to the right of the LMWL. The situation is reversed during high tide (Fig. 6b), with isotopic compositions of water from Stations 1B to 4B plotting to the right of the LMWL, as a result of mixing with sea and coastal water and all others plotting to the left (mixing with internal lagoon water, including pore water).

Two mixing lines, [MX-1: $\delta^2H = (0.97 \pm 0.08) \times \delta^{18}O + (5.70 \pm 0.09)$, $r^2 = 0.871$, $n = 21$; MX-2: $\delta^2H = (1.02 \pm 0.12) \times \delta^{18}O + (7.13 \pm 0.10)$, $r^2 = 0.842$, $n = 16$)] and an evaporation line (LEL-1: $\delta^2H = (3.88 \pm 0.26) \times \delta^{18}O + (3.26 \pm 0.27)$, $r^2 = 0.969$, $n = 9$) are defined by the paired $\delta^{18}O$ and δ^2H values of the surface and pore waters at low tide (Fig. 6a). The MX-1 line represents the isotopic composition of pore water taken from the deeper section (2–3.5 m below the sediment surface) of the beach water table (Fig. 5) and surface waters from Station 2B in the Ramalhete Channel, the outer eastern sector locations in the lagoon (Stations A–E and J, Fig. 1) and water from the Faro channel (Stations 1–4, Fig. 1). The MX-2 line represents the isotopic composition of pore water taken from the shallower section (0.5–1.5 m) below the sediment surface) of the beach water table (Fig. 5) and surface waters of the Ramalhete Channel (1B, Fig. 1), the Ancão channel close to the inlet (Stations 3B–5B, Fig. 1) and the landward stations of the eastern sector (Stations F–H, Fig. 1). LEL-1 describes all isotopic signatures of water collected in the eastern sector and intersects the LMWL amongst the most depleted pore water samples extracted from the beach (Fig. 6a) corresponding to the unsaturated zone. During high tide, water found at Stations A, B and C (Fig. 1) retains similar isotopic compositions (Fig. 6b) to the water mass found at the same locations during low tide (Fig. 6a).

HESSD

12, 12433–12482, 2015

5 Discussion

5.1 Radon source attribution

In order to derive an SGD rate for the Ria Formosa we divide the end-member source activity by the advective radon flux ($4.14 \pm 3.00 \times 10^8$ Bq day^{-1}) calculated from the mass balance. However, because radon budgets include ^{222}Rn sourced in seawater recirculation, the discharging fluid composition is important to discriminate between potential source functions of SGD. In fact the two modes of SGD may be separated according to whether they drive a net influx of freshwater to the system (Santos et al., 2012). Indeed, there are three identified potential source functions for advective radon input to the lagoon, i.e. Table 1, water in freshwater lenses under the outer barrier islands (outer reaches of the M12 aquifer) represented by the Deserta well (mean 0.95 salinity), porewater in sandy beaches (mean 40.6 salinity) mobilized by tidal pumping (seawater recirculation), and finally, meteoric water travelling through the subterranean pathway (M12 aquifer), represented by samples taken from the Ramalhete borehole (mean 5.06 salinity). The corresponding volumetric discharges, if each of these potential sources is considered in turn are $4.42\,(\pm 4.25) \times 10^6$, $1.36\,(\pm 1.28) \times 10^6$ and $6.26\,(\pm 4.63) \times 10^4$ m^3 day^{-1}, corresponding respectively to ~ 4.2, ~ 1.3 and ~ 0.1 % of the mean daily flood prism (1.04×10^8 m^3). When defining the radon source function, salinity is occasionally used as the discriminating parameter because of its conservative nature (Crusius et al., 2005; Swarzenski et al., 2006; Stieglitz et al., 2010). Yet, the low estimated SGD to tidal prism ratio combined with saline intrusion into the local aquifers (Silva et al., 1986; Table 1) advises against this option as the estimated discharge volumes would not have a discernable impact on the overall salinity of the Ria Formosa, leaving us without a way in which to verify the reliability of the choice. Furthermore, porewater salinity at the site where the piezometer transect is located (Fig. 1) was always very high during 2009–2011 (> 35; Table S1) but could be as low as 21 in 2007, suggesting different SGD modes might be active in different years. *So how do we confidently identify the source of radon?*

HESSD
12, 12433–12482, 2015

Our mass balances (see Sect. 4.1.3) for each tidal stage suggest that radon is removed from the water column during the flood period. In the absence of any other realistic explanation we might accept that it had to be advected into the unsaturated intertidal zone during beach recharge. The daily flux of radon into unsaturated sandy sediments would then amount to $16.25 \pm 13.5\,\mathrm{Bq\,m^{-2}\,day^{-1}}$. Conversely, the input of radon into the water column during ebb was $23.4 \pm 19.4\,\mathrm{Bq\,m^{-2}\,day^{-1}}$. Because the mean radon inventory during high tide was $19.3 \pm 4.74\,\mathrm{Bq\,m^{-3}}$, a flux of $16.25 \pm 13.5\,\mathrm{Bq\,m^{-2}\,day^{-1}}$ into unsaturated sediments would equate to a beach recharge rate of $\sim 1.2\,\mathrm{m\,day^{-1}}$. This figure is consistent with the discharge rates measured in 2006–2007 by Leote et al. (2008) at the lower intertidal, which reached $1.9\,\mathrm{m\,day^{-1}}$. If we therefore assume that beach discharge balances recharge on a volumetric basis at daily timescales, then the area of water infiltration would be $\sim 1.13 \times 10^6\,\mathrm{m^2}$. Given the porosity of sandy beach sediments on site of ∼ 0.3–0.4 (Rocha et al., 2009), recharge would only occur through about 7.5–10 % of the maximum surface intertidal area of the lagoon (see Sect. 2.1). Hence tidal pumping is a realistic explanation for the radon advected into the water column on a daily basis. Still, the radon data alone does not provide irrefutable proof that SGD estimated through the radon mass balance for 2009–2010 originates from seawater recirculation through beaches and pore water exchange mechanisms.

This proof is important: an example of how an unsupported choice of radon end member might significantly affect quantification of nitrate loading to the lagoon through SGD could be given at this stage to illustrate the effects of the lack of irrefutable source attribution. The mean nitrate concentration (in $\mathrm{mg\,L^{-1}}$, spring tides, 2009/11) was 0.1 for the lagoon water column, 0.81 for beach pore waters, 2.22 in the Deserta well, and 130 for the Campina de Faro aquifer (M12). Our discharge estimates based on the radon balance would then result in potential average SGD borne nitrate loading to the Ria Formosa of 0.96, 9.8 and $8.14\,\mathrm{t\,N\,day^{-1}}$, if the source of excess radon was respectively seawater recirculation through beach sands or fresh groundwater originating from either the lens under the dune cordon or the landward section of M12 aquifer. Two cautionary notes on these numbers should be obvious: (a) the latter would drive net additions to the lagoon water budget while the former would not, implying that (b) the loadings based on directly multiplying fresh SGD by the average nutrient concentrations found in the end member samples ignore any transformations occurring within the interface before the mixture arrives at the lagoon proper, and therefore are likely to be overestimated.

Ferreira et al. (2003) estimated total N fluxes to the lagoon at $1028\,\mathrm{t\,N\,yr^{-1}}$ ($2.82\,\mathrm{t\,N\,day^{-1}}$), with 58 % ($1.64\,\mathrm{t\,N\,day^{-1}}$) originating from diffuse sources. Simple extrapolation from our data would suggest that ~ 34 % of the total N fluxes to the lagoon, and ~ 59 % of the non-point source loading, would arise from seawater recirculation through beaches, while the meteoric SGD sources would multiply the total N loading into the system by a factor of 6 or 5 on a daily basis, depending on the composition of fresh groundwater. These two latest figures compound our cautionary notes above. Furthermore, during 2009–2011, when pore water salinities were very high, nitrate available in pore waters at the littoral fringe is likely sourced from benthic mineralization of local organic matter (autochthonous source) and not in fresh groundwater input. Conversely, because nitrate contamination of the Campina de Faro aquifer is anthropogenic, freshwater inflow via SGD into the lagoon would also define the associated nitrate inputs as allochthonous, or "new" contributions to the system's nutrient budget. Depending on SGD source therefore, there would be an order of magnitude difference between allochthonous and autochthonous sources of nitrate into the lagoon, even if the former might be overestimated as discussed. Accurately identifying the SGD source function would therefore be absolutely necessary to understand the biogeochemical workings of the lagoon, but this is not possible with the radon data alone, even in combination with the salinity data.

However, the stable isotope signatures of surface water bring clarity to the problem. The Local Evaporation Line (LEL-1, Fig. 6a) fitted by linear regression of the samples taken within the eastern sector at low tide intersects the LMWL close to the average isotopic signature of beach pore water in the unsaturated zone (Figs. 5a and 6a). This indicates the original composition of the surface water before evaporation and mixing takes place within the lagoon. The origin of the surface water is the recharge into the unsaturated beach area, which then reveals isotopic enrichment in proportion to its permanence within the system and the consequent extent of evaporative loss. Indeed, water in the upper intertidal at low tide will see its isotopic signature depleted within the sedimentary matrix – in the unsaturated zone, the isotopic concentration decreases quickly from a maximum at the zone of evaporation (phreatic surface) within the sediment matrix to a minimum close to the surface because of the movement of water vapor through the pores toward the surface (Barnes and Allison, 1983, 1988). While this is clear for the eastern sector, within the western sector there is another surface source of water that further complicates the picture. This source of water joins the lagoon close to Station 2B (Fig. 6a). So, the pore water in the unsaturated sediments mixes over time with the lagoon recharge at high tide and water already present within the tidal wedge (cf. Robinson et al., 2007), whereupon it leaves during beach discharge at low tide, either through shallow or deeper flow paths (Fig. 5b) and mixes with other meteoric sources and seawater (MX-1, MX-2, Fig. 6a).

For 2009–2010 therefore, the combined stable isotope and radon tracer approach allows definite attribution of the SGD source into the Ria Formosa. SGD arises from seawater recirculation through the permeable beach sediments of the lagoon driven by the tide. In the absence of meteoric SGD inputs, a significant amount of the tidal prism (1.3 %) circulates through local sandy sediments driven by tidal pumping, at a rate of $\sim 1.4 \times 10^6\ m^3\ day^{-1}$. This implies that the entire tidal-averaged volume of the lagoon ($140 \times 10^6\ m^3$) is filtered through its sandy beaches within 100 days, or about 3.5 times a year. Based on our nutrient data, the average nitrate loading driven by this SGD mode to the Ria Formosa can now be confidently put at an average of $0.96\ t\,N\,day^{-1}$, $\sim 59\,\%$ of the non-point source nitrogen loading estimated by Ferreira et al. (2003).

Salinity (see Table S1) does not correlate well with both $\delta^{18}O$ and δ^2H, though, particularly for samples with $\delta^{18}O > 1\,‰$ and/or $\delta^2H > 1$ and $S > 37\,‰$. With reference to surface water $\delta^{18}O$ values these comprise the most isotopically enriched waters found

HESSD
12, 12433–12482, 2015

during low tide respectively the innermost stations in the eastern sector (Stations G, H and F; Figs. 1 and 6a) and at locations within the Faro channel (Stations 1–4; Figs. 1 and 6a) as discussed earlier. It is also the case for most pore water samples. Indeed, even if the mean composition of pore water from different sections of the beach plot along well-defined mixing and evaporation lines (Fig. 5a and b), the average salinities of each group do not change significantly with $\delta^{18}O$ enrichment (40.2 ± 1.78, 40.6 ± 2.57 and 40.6 ± 2.07 respectively). While this observation is consistent with theory (Craig and Gordon, 1965) and previous analysis on the covariance of $\delta^{18}O$, $\delta^{2}H$ and salinity in seawater (Rohling, 2007), it also implies that the joint use of these tracers to infer the relative contribution of different source functions has to be done with care in semi-confined coastal water bodies subject to significant evaporation. As further support to this observation, we note that the mixing lines (MX-1 and MX-2, Fig. 6a) between the porewater within the beach tidal wedge and the most enriched waters found in the western sector ($\delta^2H = (0.97 \pm 0.08) \times \delta^{18}O + (5.70 \pm 0.09)$, $r^2 = 0.87$, $n = 21$) and between the Ramalhete Channel and Ancão Basin (Stations 3B, 4B, 5B) and the water mass near Olhão at Stations G and H ($\delta^2H = (1.02 \pm 0.18) \times \delta^{18}O + (7.13 \pm 1.01)$, $r^2 = 0.84$, $n = 16$) are virtually the same as that characteristic of the modern surface ocean ($\delta^2H = 1.05 \times \delta^{18}O + 6.24$, $r^2 = 0.21$, $n = 62$) within a comparable salinity range (Rohling, 2007). This observation suggests in coastal ocean regions and areas of restricted exchange like lagoons, the stable isotope signature of seawater reflects important contributions arising from pore-water exchange driven by tidal pumping, amongst other mechanisms. Identifying and discriminating these contributions brings insights also into the hydrological paths active within these systems and therefore provides an invaluable tool to support reliable biogeochemical budgets.

5.2 Hydrological pathways and dispersion of SGD in the Ria Formosa Lagoon

The amount-weighed isotopic composition of precipitation over Faro (GNIP: IAEA/WMO, 2013) plots (Fig. 4a) at the intercept point of the GMWL, the LMWL (slope ~ 6.4) and the precipitation-seawater mixing line (slope ~ 5.4). The isotopic signature of precipitation hence plots close to that of groundwater, indicating that local aquifers are directly recharged by precipitation, in agreement with prior reports (Engelen and van Beers, 1986). The isotopic composition of surface waters also reveals that the lagoon and the adjacent coastal water may be classified as a coastal boundary zone similar to that described elsewhere (Blanton et al., 1989, 1994; Moore, 2000), in which the isotopic signatures result from the mixing between offshore seawater and continental meteoric sources affected by surface evaporation.

Accordingly (Fig. 6), the stable isotope composition of water within the lagoon varies with tidal stage and will be affected on the one hand by the magnitude, origin and pathways taken by the meteoric inputs and on the other by internal mixing, driven by lagoon hydrodynamics and by the local evaporation regime. Nevertheless, the pore water end-member is part of the surface water mixture on both sampled periods, although in different ways: some porewaters (Pw_e and Pw_f; see Table S1) collected at the same site were significantly more depleted in both ^{18}O and ^{2}H during 2007 (Fig. 4b) when compared to 2009–2011 (Fig. 4c) and these are characterized by comparatively low salinities (21 and 23, Table S1). Station 2B is the closest to the Faro WWTP outlet; during low tide the water mass joining the lagoon mixture there has an isotopic signature close to the Western Mediterranean Water Line (Fig. 6a), suggesting that a meteoric source of water joins the lagoon there presumably as part of the WWTP discharge. On the other hand, the exchange in position of the isotopic signature of water at Stations 1–5 and 1B–3B with reference to the LMWL in $\delta^{18}O - \delta^{2}H$ space during flood (Fig. 6b) suggests a hydrodynamic connection between the Ramalhete Channel and the Ancão inlet and the water masses on the eastern sector, both the ones closest to the city of Olhao (Stations E, F, G) and the ones closer to the coastal ocean (Stations A, B, C), via the Faro-Olhão inlet and associated channels as ebb progresses onto flood. Indeed, Stations 1 to 4 in the Faro channel display depletion of ^{18}O during high tide (Fig. 6b) by comparison to low tide (Fig. 6a). This provides evidence that the meteoric source present within the Ramalhete channel also influences the water in the Faro channel during high tide. Furthermore, the isotopic data suggest that part of the wa-

HESSD
12, 12433–12482, 2015

Assessing land–ocean connectivity via SGD in the Ria Formosa Lagoon

C. Rocha et al.

ter mass out flowing through the Ramalhete channel during ebb tide (Stations 2B–5B) eventually end up being present at Stations F, G and H close to the city of Olhão via the inner portion of the system (Station 1B), having mixed with shallow beach groundwater (MX-2 in Fig. 6a) while water from the same region might also be led to Stations A, B and C in the eastern sector via Station 5 after mixing through the beach water table (MX-1 in Fig. 6a and b). The dominant alongshore drift in the area is eastward, and in fact, Pacheco et al. (2010) show that a strong hydraulic connection exists between the the Ancão, Barra Nova (Faro-Olhão) and Armona (Barra Velha) inlets, whereby the excess flood prism at Barra Nova is directed toward both the Ancão and the Armona ebb-dominated inlets. The combination of data indicates that the body of water ebbing in the first instance through the Ramalhete channel is partially retained within the system and ends up in the Faro channel before the subsequent flood moves it eastward, either via an internal pathway eastward from the Ancão inlet basin and/or externally, looping back into the lagoon via the Faro-Olhão inlet after exiting through the Ancão inlet (Fig. 6a and b).

The combination of flood lag-time between the Ancão and Barra Nova inlets, the eastward alongshore drift and the meteoric source of water at the WWTP plant outlet (closest to Station 2B) creates the characteristic inversion observed in $\delta^{18}O$–$\delta^{2}H$ relationships and highlighted in Fig. 6a and b. This circulation path inferred from the isotopic composition of water is also consistent with the radon data, since the radon enriched water masses found in the Ramalhete and Faro channels (Fig. 2a) during low tide would eventually be transported toward the eastern sector via the distribution of the excess flood prism at Faro-Olhão (Pacheco et al., 2010). This would help explain why the radon inventory in the eastern sector is higher during flood tide (Fig. 2b), and why the net exchange of radon is directed into the lagoon at both Quatro-Águas and Barra Nova (Table 1), as part of the radon associated with beach seepage would be retained in the lagoon and/or transported back into the system via the Barra-Nova after exiting through the Ancão inlet.

5.3 Inter-annual comparison of lagoon hydrology using Deuterium excess

Because of the relatively higher enrichment in ^{18}O compared to ^{2}H in the residual water (Gat, 1996), deuterium excess (*d-excess* = $d = \delta^2\text{H} - 8 \times \delta^{18}\text{O}$) decreases in water as evaporation progresses (i.e. as δ^{18}O increases). It follows therefore that a plot of *d-excess* vs. δ^{18}O (in a similar fashion to Fig. 5b for porewater) might reveal the path taken by a particular water mass within a catchment area, because, (a) the magnitude of the fractionation imposed by evaporation along the travel path affects the *d-excess* of residual water (setting the slope of paired $d - \delta^{18}\text{O}$ relationships), and (b) water of different origins would have different *d-excess* values. The slope of the $d - \delta^{18}\text{O}$ covariance line shows the deviation of isotopic compositions from Craig's meteoric water line (Craig, 1961b). Therefore its magnitude in absolute terms is proportional to the extent of evaporative enrichment, a function of the exposure time of the water to evaporation. Conversely, following the line along decreasing δ^{18}O values would lead us to the original isotopic composition of the water, set before the evaporative regime changed. These characteristics allow us to disentangle and identify the main hydraulic pathways active in the Ria Formosa and compare the two periods under scrutiny to reveal the distinct nature of SGD within the system (Figs. 5b and 7a and b).

Accordingly, four significant $d - \delta^{18}\text{O}$ correlation lines are identified in the basin (Fig. 7). In 2007, two pathways (P1 and P2) connecting the composition of M12 groundwater with water sampled in the lagoon are revealed: P1, with $d = (-1.10 \pm 0.02) \times \delta^{18}\text{O} + (4.41 \pm 0.1)$, $r^2 = 0.997$, $n = 6$, $P \sim 0$; and P2, with $d = (-1.85 \pm 0.05) \times \delta^{18}\text{O} + (0.72 \pm 0.11)$, $r^2 = 0.992$, $n = 14$, $P \sim 0$). These relations reveal the two different pathways into the Ria followed by groundwater from the M12 aquifer in 2007 (Fig. 7a). The surface water circulation pathway (P1) originates when water from the public supply (sourced in local aquifers) is treated at the WWTP and subsequently discharged into the lagoon, whereupon it circulates into the Ancão basin mixing with coastal and seawater. This pathway is consistent with the internal circulation path discussed earlier. In contrast, the groundwater pathway (P2) followed by water originating

HESSD
12, 12433–12482, 2015

in the same aquifer crosses the subterranean estuary and emerges later ($d-\delta^{18}O$ correlation slope magnitude is higher than P1) within the lagoon where it mixes with surface waters, including seawater and the WWTP outlet emissions (Fig. 7a). Hence the isotope data conclusively show two aspects of the local water balance in 2007: on the one hand, water for public consumption was essentially extracted from groundwater sources while on the other SGD into the lagoon comprising a net water input into the system was present.

The situation later (2009–2011) was substantially different (Fig. 7b). Two major hydraulic pathways are shown in the isotopic data (P3, P4); P3, with $d = (-7.8 \pm 1.2) \times \delta^{18}O - (22.76 \pm 5.04)$, $r^2 = 0.813$, $n = 10$, $P = 0.0002$; and P4, $d = (-7.43 \pm 0.18) \times \delta^{18}O + (6.45 \pm 0.18)$, $r^2 = 0.979$, $n = 37$, $P \sim 0$. These highlight other aspects of the local water balance. Firstly, P3 suggests that groundwater from the M10 aquifer mixes with water in M12, and that the local groundwater flow follows a Northeast to southeast general direction (cf. location of M10 and M12 in Fig. 1), eventually communicating under the Ria Formosa with freshwater lenses present in the barrier islands, where the *d-excess* signature of groundwater is lowest. Secondly, P4 shows that water used for public consumption in the catchment was mainly withdrawn from a direct meteoric source (position of rainwater signature, Fig. 7b). This water, upon leaving the WWTPs then mixes with surface and re-circulated seawater establishing the mixing line for the lagoon (Figs. 6a and 7b). It is also evident that the surface water samples collected in the lagoon in 2007 plot close to the P4 line, suggesting that the magnitudes of the factors driving evaporation and internal circulation in the lagoon are generally stable on a multiannual basis. This comparative approach confirms, additionally, that the subterranean pathway was not present in 2009–2011, and hence SGD at this time was comprised entirely of saline water re-circulated through the sandy beaches by tidal pumping.

The difference observed in water sources for public water supply and their isotopic signature in the catchment and subsequently released through the WWTPs into the lagoon is consistent with the changes occurring in the regional water management strategy: while water to meet irrigation and public consumption demand relied almost entirely on groundwater abstraction until the 2000's (Stigter et al., 2006), from this period onwards it was to be drawn almost exclusively from surface reservoirs North of the littoral zone. However, a substantial number of the local groundwater captions remained active in support of irrigation, while some of the major municipal captions had to be re-activated after the 2005 drought (EM-DAT 2013) to support consumption demand when surface reservoirs became depleted. In fact, because of the unpredictability of scarcity periods, the current operational thinking tends toward mixing both water sources to face demand, with the primary source being surface water reservoirs (Monteiro and Costa Manuel, 2004; Stigter and Monteiro, 2008). Our approach clearly indicates that this is the case for 2009–2011 as the WWTP plant water signal shows the water being discharged as meteoric in origin (Figs. 6a and 7b). Following the implementation of a mixed source water supply chain, the activity of the SGD subterranean pathway into the Ria becomes dependent on whether groundwater levels in M12 are sufficient to establish a hydraulic gradient driving the flow as was apparently the case in 2007 (Fig. 7a). Increased water mining and reduced aquifer recharge would provide the counterbalance by reducing groundwater levels and consequently the hydraulic gradient driving SGD of meteoric origin into the system via the subterranean estuary.

6 Concluding remarks

We compared hydrological scenarios in a semi-arid coastal lagoon across two different periods, aiming to distinguish SGD modes and correctly identify end-member contributions to the water mixture within the system. While it has been established that radon mass conservation allows for the determination of total SGD, i.e. meteoric plus re-circulated water flow, we show that combining this information with stable isotope hydrology contributes to define and distinguish origins and pathways followed by SGD into the system. While δ^{18}O and *d-excess* paired data helped define the active hydrological pathways in the Ria Formosa, δ^{2}H vs. δ^{18}O plots provided insights into

HESSD
12, 12433–12482, 2015

water source functions and their dispersion through the lagoon. Using our combined approach, SGD occurring in the Ria Formosa could be separated into a discharge incorporating net meteoric water input into a receiving ecosystem (2007) and an input with no net water transfer (2009–2011). We conclude that whilst the Ria Formosa receives SGD through tidal pumping (as in 2009–2011), it is also occasionally subject to SGD inputs of meteoric origin (as in 2007) directly associated with the contaminated M12 aquifer.

In the absence of meteoric SGD inputs part of the tidal prism (1.3 %) circulates through local sandy sediments driven by tidal pumping, at a rate of $\sim 1.4 \times 10^6\,m^3\,day^{-1}$. This implies that the entire tidal-averaged volume of the lagoon ($140 \times 10^6\,m^3$) is filtered through its sandy beaches within 100 days, or about 3.5 times a year, driving an estimated load of $\sim 350\,t\,N\,yr^{-1}$ into the lagoon. Conversely, using the estimates for the upper bound of N concentration found in the freshwater component of SGD during 2006 ($0.4\,mmol\,L^{-1}$) and the associated SGD-borne freshwater discharge of $\sim 1.1 \times 10^7\,m^3\,yr^{-1}$ estimated by Leote et al. (2008) based on seepage meter measurements, meteoric SGD inputs could add a further $\sim 61\,t\,N\,yr^{-1}$ to the lagoon. If for the former the source is autochthonous and responsible for a rather large fraction (59 %) of the estimated nitrogen inputs into the system via non-point sources (Ferreira et al., 2003), leaving no direct mitigation options in the context of environmental management – it is not so for the latter, as specific measures could be implemented in support of mitigation (e.g. Almasri and Kaluarachchi, 2004). Nevertheless, the potential loadings delivered from two distinct vectors differ in magnitude, frequency and origin, and could therefore cause different ecosystem-level impacts. Hence while simple or weighed averages of end member radon activities might be useful under well defined circumstances (Crusius et al., 2005; Swarzenski et al., 2006; Kroeger et al., 2007; Blanco et al., 2011) in radon budgets to evaluate SGD as a potential pollutant source in comparison to other vectors (local surface drainage, riverine input, etc.), these are of little value to effectively provide environmental managers with the causal chain alluded

HESSD
12, 12433–12482, 2015

to in the introduction: without actual source identification and attribution, there is little that can be done to manage potential pollutant loading of coastal ecosystems via SGD.

The Supplement related to this article is available online at doi:10.5194/hessd-12-12433-2015-supplement.

Acknowledgements. Funding for this study was provided by the Portuguese Foundation for Science and Technology (FCT), the EU (FEDER) and the Portuguese Government through project NITROLINKS – "NITROgen loading into the Ria Formosa through Coastal Groundwater Discharge (CGD) – Pathways, turnover and LINKS between land and sea in the Coastal Zone" (PTDC/MAR/70247/2006). J. Wilson was funded by the Environmental Protection Agency (EPA) Ireland under the STRIVE initiative (project code 2008-FS-W-S5). J. Scholten acknowledges the support provided by the FP7 EU Marie Curie Career Integration Grant (grant PCIG09-GA-2011-293499). Numerous people helped at various stages of the work. In particular, the authors wish to thank Inês Rio, Rachel Kilgallon, Collin Snowberg, Sinead Kehoe and Aine Kenny, for their help with the field surveys and laboratory analysis. The pilots of our survey boats, Daniel Machado, Pedro Barroso and the Animaris crews are gratefully acknowledged – their profound knowledge of the system and their piloting proficiency made the impossible possible.

References

Almasri, M. N. and Kaluarachchi, J. J.: Assessment and management of long-term nitrate pollution of ground water in agriculture-dominated watersheds, J. Hydrol., 295, 225–245, 2004.

Almeida, C. and Silva, M. L.: Incidence of agriculture on water quality at Campina de Faro (south Portugal), in: Hidrogeologia-y-Recursos-Hidraulicos, vol. 12, Associacion Española de Hidrologia Subterranea, Madrid, Spain, 249–257, 1987.

Almeida, C. J., Mendonca, J. J. L., Jesus, M. R., and Gomes, A. J.: Sistemas aquiferos de Portugal Continental (Aquifer Systems of Continental Portugal), Instituto Nacional da Água – INAG, Lisbon, 2000.

HESSD
12, 12433–12482, 2015

Assessing land–ocean connectivity via SGD in the Ria Formosa Lagoon

C. Rocha et al.

Balouin, Y.: Les embouchures mésotidales (tidal inlets) et leur relation avec les littoraux adjacents – exemple de la Barra Nova, sud Portugal, PhD thesis, University of Bordeaux, Boredeaux, 2001.
Barnes, C. J. and Allison, G. B.: The distribution of deuterium and ^{18}O in dry soils: 1. Theory, J. Hydrol., 60, 141–156, 1983.
Barnes, C. J. and Allison, G. B.: Tracing of water movement in the unsaturated zone using stable isotopes of hydrogen and oxygen, J. Hydrol., 100, 143–176, 1988.
Beck, A. J., Tsukamoto, Y., Ovar-Sanchez, A., Huerta-Diaz, M., Bokuniewicz, H. J., and Sañudo-Wilhelmy, S. A.: Importance of geochemical transformations in determining submarine groundwater discharge-derived trace metal and nutrient fluxes, Appl. Geochem., 22, 477–490, 2007.
Blanco, A. C., Watanabe, A., Nadaoka, K., Motooka, S., Herrera, E. C., and Yamamoto, T.: Estimation of nearshore groundwater discharge and its potential effects on a fringing coral reef, Mar. Pollut. Bull., 62, 770–785, 2011.
Blanton, J. O., Amft, J., Oey, L.-Y., and Lee, T. N.: Advection of momentum and buoyancy in a coastal frontal zone, J. Phys. Oceanogr., 19, 98–115, 1989.
Blanton, J. O., Werner, F., Kim, C., Atkinson, L., Lee, T., and Savidge, D.: Transport and fate of low-density water in a coastal frontal zone, Cont. Shelf. Res., 14, 401–427, 1994.
Bratton, J. F.: The three scales of submarine groundwater flow and discharge across passive continental margins, J. Geol., 118, 565–575, 2010.
Burnett, W. C. and Dulaiova, H.: Estimating the dynamics of groundwater input into the coastal zone via continuous radon-222 measurements, J. Environ. Radioactiv., 69, 21–35, 2003.
Burnett, W. C., Taniguchi, M., and Oberdorfer, J.: Measurement and significance of the direct discharge of groundwater into the coastal zone, J. Sea Res., 46, 109–116, 2001a.
Burnett, W. C., Kim, G., and Lane-Smith, D.: A continuous monitor for assessment of ^{222}Rn in the coastal ocean, J. Radioanal. Nucl. Ch., 249, 167–172, 2001b.
Burnett, W. C., Bokuniewicz, H., Huettel, M., Moore, W. S., and Taniguchi, M.: Groundwater and pore water inputs to the coastal zone, Biogeochemistry, 66, 3–33, 2003.
Burnett, W. C., Aggarwal, P. K., Aureli, A., Bokuniewicz, H., Cable, J. E., Charette, M. A., Kontar, E., Krupa, S., Kulkarni K. M., Loveless, A., Moore, W. S., Oberdorfer, J. A., Oliveira, J., Ozyurt, N., Povinec, P., Privitera, A. M., Rajar, R., Ramessur, R. T., Scholten, J., Stieglitz, T., Taniguchi, M., and Turner, J. V.: Quantifying submarine groundwater discharge in the coastal zone via multiple methods, Sci. Total Environ., 367, 498–543, 2006.

HESSD
12, 12433–12482, 2015

Assessing land–ocean connectivity via SGD in the Ria Formosa Lagoon

C. Rocha et al.

Burnett, W. C., Peterson, R., Moore, W. S., and de Oliveira, J.: Radon and radium isotopes as tracers of submarine groundwater discharge – results from the Ubatuba, Brazil SGD assessment intercomparison, Estuar. Coast. Shelf S., 76, 501–511, 2008.
Cable, J. E., Burnett, W. C., Chanton, J. P., and Weatherly, G. L.: Estimating groundwater discharge into the northeastern Gulf of Mexico using radon-222, Earth Planet. Sc. Lett., 144, 591–604, 1996.
Cable, J. E., Martin, J. B., Swarzenski, P. W., Lindenberg, M. K., and Steward, J.: Advection within shallow pore waters of a coastal lagoon, Florida, Ground Water, 42, 1011–1020, 2004.
Carpenter, S. R., Caraco, N. F., Correll, D. L., Howarth, R. W., Sharpley, A. N., and Smith, V. H.: Nonpoint pollution of surface waters with phosphorus and nitrogen, Ecol. Appl., 8, 559–568, 1998.
Carreira, P. M.: Mechanisms of Salinization of Coastal Aquifers in the Algarve, MSc thesis, ICEN/INETI, 143 pp., 1991.
Carreira, P. M., Araújo, M. F., and Nunes, D.: Isotopic composition of rain and water vapour samples from Lisbon region: characterization of monthly and daily events, in: Isotopic Composition of Precipitation in the Mediterranean Basin in Relation to Air Circulate Patterns and Climate, IAEA-TECDOC-1453, IAEA, Vienna, Austria, 141–156, 2005.
Celle-Jeanton, H., Travi, Y., and Blavoux, B.: Isotopic typology of the precipitation in the western Mediterranean region at three different time scales, Geophys. Res. Lett., 28, 1215–1218, 2001.
Charette, M. A. and Sholkovitz, E. R.: Trace element cycling in a subterranean estuary: Part 2. Geochemistry of the pore water, Geochim. Cosmochim. Acta, 70, 811–826, 2006.
Charette, M. A., Sholkovitz, E. R., and Hansel, C. M.: Trace element cycling in a subterranean estuary: Part 1. Geochemistry of the permeable sediments, Geochim. Cosmochim. Acta, 69, 2095–2109, 2005.
Church, T. M.: An underground route for the water cycle, Nature, 380, 579–580, 1996.
Clark, I. D. and Fritz, P.: Environmental Isotopes in Hydrogeology, CRC Press, Boca Raton, Florida, 1997.
Colbert, S. L. and Hammond, D. E.: Temporal and spatial variability of radium in the coastal ocean and its impact on computation of nearshore cross-shelf mixing rates, Cont. Shelf. Res., 27, 1477–1500, 2007.
Colbert, S. L. and Hammond, D. E.: Shoreline and seafloor fluxes of water and short-lived Ra isotopes to surface water of San Pedro Bay, CA, Mar. Chem., 108, 1–17, 2008.

Colbert, S. L., Hammond, D. E., and Berelson, W. M.: Radon-222 budget in Catalina Harbor, California: 1. Water mixing rates, Limnol. Oceanogr., 53, 651–658, 2008a.
Colbert, S. L., Berelson, W. M., and Hammond, D. E.: Radon-222 budget in Catalina Harbor, California: 2. Flow dynamics and residence time in a tidal beach, Limnol. Oceanogr., 53, 659–665, 2008b.
Corbett, D. R., Burnett, W. C., Cable, P. H., and Clark, S. B.: A multiple approach to the determination of radon fluxes from sediments, J. Radioanal. Nucl. Ch., 236, 247–253, 1998.
Craig, H.: Standard for reporting concentrations of deuterium and oxygen-18 in natural waters, Science, 133, 1833–1834, 1961a.
Craig, H.: Isotopic variations in meteoric waters, Science, 133, 1702–1703, 1961b.
Craig, H. and Gordon, L. I.: Deuterium and oxygen-18 variations in the ocean and the marine atmosphere, in: Proceedings of a Conference on Stable Isotopes in Oceanographic Studies and Paleotemperatures, Spoleto, Italy, edited by: Tongiorgi, E., 9–130, 1965.
Crusius, J., Koopmans, D., Bratton, J. F., Charette, M. A., Kroeger, K., Henderson, P., Ryckman, L., Halloran, K., and Colman, J. A.: Submarine groundwater discharge to a small estuary estimated from radon and salinity measurements and a box model, Biogeosciences, 2, 141–157, doi:10.5194/bg-2-141-2005, 2005.
Dansgaard, W.: Stable isotopes in precipitation, Tellus, 16, 436–468, 1964.
Dias, J. M. and Sousa, M. C.: Numerical modeling of Ria Formosa tidal dynamics, J. Coast. Res., 56, 1345–1349, 2009.
Edmunds, W. M.: Renewable and non-renewable groundwater in semi-arid and arid regions, in: Developments in Water Science, Vol. 50, edited by: Alsharhan, A. S. and Wood, W. W., Elsevier, Amsterdam, 265–280, 2003.
EM-DAT: The OFDA/CRED International Disaster Database, available at: www.emdat.be (last access: June 2013), Université Catholique de Louvain, Brussels, Belgium, 2013.
Engelen, G. B. and van Beers, P. H.: Groundwater systems in the eastern Algarve, Portugal, in: Developments in the Analysis of Groundwater Flow Systems, IAHS Red Book Series 163, edited by: Engelen, G. B. and Jones, G. P., UNESCO/IAHS, Wallingford, UK, 325–331, 1986.
Ferreira, J. G., Simas, T., Nobre, A., Silva, M. C., Shifferegger, K., and Lencart-Silva, J.: Identification of Sensitive Areas and Vulnerable Zones in Transitional and Coastal Portuguese Systems, Instituto da Água and Institute of Marine Research, 168 pp., available at: http://www.eutro.org/documents/NEEAPortugal.pdf, 2003.

HESSD
12, 12433–12482, 2015

Finkl, C. W. and Krupa, S. L.: Environmental impacts of coastal-plain activities on sandy beach systems: hazards, perception and mitigation, J. Coast. Res., SI 35, 132–150, 2003.
Frot, E., van Wesemael, B., Vandenschrick, G., Souchez, R., and Benet, A. S.: Origin and type of rainfall for recharge of a karstic aquifer in the western Mediterranean: a case study from the Sierra de Gador–Campo de Dalias (southeast Spain), Hydrol. Process., 21, 359–368, 2007.
Gat, J. R.: Oxygen and hydrogen isotopes in the hydrologic cycle, Annu. Rev. Earth Pl. Sc., 24, 225–262, 1996.
Gat, J. R. and Carmi, I.: Evolution of the isotopic composition of atmospheric waters in the Mediterranean Sea area, J. Geophys. Res., 75, 3039–3048, 1970.
Gat, J. R., Bowser, C. J., and Kendall, C.: The contribution of evaporation from the Great Lakes to the continental atmosphere: estimate based on stable isotope data, Geophys. Res. Lett., 21, 557–560, 1994.
Gibson, J. J. and Edwards, T. W. D.: Regional water balance trends and evaporation–transpiration partitioning from a stable isotope survey of lakes in northern Canada, Global Biogeochem. Cy., 16, 10–11, 2002.
Gonneea, M. E., Morris, P. J., Dulaiova, H., and Charette, M. A.: New perspectives on radium behavior within a subterranean estuary, Mar. Chem., 109, 250–267, 2008.
Hampel, F. R.: The influence curve and its role in robust estimation, J. Am. Stat. Assoc., 69, 383–393, 1974.
Hancock, G. J. and Murray, A. S.: Source and distribution of dissolved radium in the Bega River Estuary, southeastern Australia, Earth Planet. Sc. Lett., 138, 145–155, 1996.
Hancock, G. J., Webster, I. T., Ford, P. W., and Moore, W. S.: Using Ra isotopes to examine transport processes controlling benthic fluxes into a shallow estuarine lagoon, Geochim. Cosmochim. Acta, 64, 3685–3699, 2000.
IAEA/WMO: Global Network of Isotopes in Precipitation, The GNIP Database, available at: http://www.iaea.org/water (last access: June 2014), 2013.
Ibánhez, J. S. P., Leote, C., and Rocha, C.: Porewater nitrate profiles in sandy sediments hosting submarine groundwater discharge described by an Advection–Dispersion-Reaction Model, Biogeochemistry, 103, 159–180, 2011.
Ibánhez, J. S. P., Leote, C., and Rocha, C.: Seasonal enhancement of Submarine Groundwater Discharge (SGD) – derived nitrate loading into the Ria Formosa coastal lagoon assessed by 1-D modeling of benthic NO_3-profiles, Estuar. Coast. Shelf S., 132, 56–64, 2013.

IH – Instituto Hidrografico: Marés 81/82 Ria de Faro. Estudo das marés de oito estações da Ria de Faro, Rel. FT-MC-4/86, IH – Instituto Hidrografico, Lisbon, 1986.
Kjerfve, B.: Comparative oceanography of coastal lagoons, in: Estuarine Variability, edited by: Wolfe, D. A., Academic Press, New York, 63–81, 1986.
Kroeger, K. D., Swarzenski, P. W., Greenwood, W. J., and Reich, C.: Submarine groundwater discharge to Tampa Bay: nutrient fluxes and biogeochemistry of the coastal aquifer, Mar. Chem., 104, 85–97, 2007.
Lee, D. R.: A device for measuring seepage flux in lakes and estuaries, Limnol. Oceanogr., 22, 140–147, 1977.
Leote, C., Ibánhez, J. S., and Rocha, C.: Submarine groundwater discharge as a nitrogen source to the Ria Formosa studied with seepage meters, Biogeochemistry, 88, 185–194, 2008.
Li, L., Barry, D. A., Stagnitti, F., and Parlange, J.-Y.: Submarine groundwater discharge and associated chemical input to a coastal sea, Water Resour. Res., 35, 3253–3259, 1999.
Lobo-Ferreira, J. P., Oliveira, M. M., Diamantino, C., and Leitão, T. E.: LNEC Contribution to D24: AR needs in Campina de Faro, Julho, LNEC, Lisbon, 6 pp., 2007.
Macintyre, S., Wanninkhof, R., and Chanton, J. P.: Trace gas exchange across the air–sea interface in freshwater and coastal marine environments, in: Biogenic Trace Gases: Measuring Emissions from Soil and Water, edited by: Matson, P. A. and Harris, R. C., Blackwell Science Ltd, Cambridge, MA, 52–97, 1995.
Martin, J. B., Cable, J. E., Swarzenski, P. W., and Lindenberg, M. K.: Enhanced submarine ground water discharge from mixing of pore water and estuarine water, Ground Water, 42, 1000–1010, 2004.
Michael, H. A., Mulligan, A. E., and Harvey, C. F.: Seasonal oscillations in water exchange between aquifers and the coastal ocean, Nature, 436, 1145–1148, 2005.
Monteiro, J. P. and Costa Manuel, S.: Dams groundwater modelling and water management at the regional scale in a coastal Meditrranean area (the southern Portugal Region – Algarve), Larhyss J., 3, 157–169, 2004.
Moore, W. S.: Large groundwater inputs to coastal waters revealed by ^{226}Ra enrichments, Nature, 380, 612–614, 1996.
Moore, W. S.: The subterranean estuary: a reaction zone of ground water and sea water, Mar. Chem., 65, 111–125, 1999.

Moore, W. S.: Determining coastal mixing rates using radium isotopes, Cont. Shelf. Res., 20, 1993–2007, 2000.
Moore, W. S.: The role of submarine groundwater discharge in coastal biogeochemistry, J. Geochem. Explor., 88, 389–393, 2006.
Moore, W. S.: The effect of submarine groundwater discharge on the ocean, Annu. Rev. Mar. Sci., 2, 59–88, 2010.
Moore, W. S. and Arnold, R.: Measurement of ^{223}Ra and ^{224}Ra in coastal waters using a delayed coincidence counter, J. Geophys. Res.-Oceans, 101, 1321–1329, 1996.
Moore, W. S. and Church, T. M.: Submarine groundwater discharge, Nature, 382, p. 122, 1996.
Mudge, S. M., Icely, J. D., and Newton, A.: Residence times in a hypersaline lagoon: using salinity as a tracer, Land Ocean Interactions in the Coastal Zone, LOICZ: Lessons from Banda Aceh, Atlantis, and Canute, Estuar. Coast. Shelf S., 77, 278–284, 2008.
Mulligan, A. E. and Charette, M. A.: Intercomparison of submarine groundwater discharge estimates from a sandy unconfined aquifer, J. Hydrol., 327, 411–425, 2006.
Munksgaard, N. C., Wurster, C. M., Bass, A., Zagorskis, I., and Bird, M. I.: First continuous shipboard δ^{18}O and δD measurements in sea water by diffusion sampling – Cavity Ring-Down Spectrometry, Environ. Chem. Lett., 10, 301–307, 2012.
Pacheco, A., Ferreira, Ó., Williams, J. J., Garel, E., Vila-Concejo, A., and Dias, J. A.: Hydrodynamics and equilibrium of a multiple-inlet system, Mar. Geol., 274, 32–42, 2010.
Prieto, C. and Destouni, G.: Is submarine groundwater discharge predictable?, Geophys. Res. Lett., 38, L01402, doi:10.1029/2010GL045621, 2010.
Robinson, C., Li, L., and Barry, D. A.: Effect of tidal forcing on a subterranean estuary, Adv. Water Resour., 30, 851–865, 2007.
Rocha, C., Ibanhez, J., and Leote, C.: Benthic nitrate biogeochemistry affected by tidal modulation of Submarine Groundwater Discharge (SGD) through a sandy beach face, Ria Formosa, southwestern Iberia, Mar. Chem., 115, 43–58, 2009.
Rodgers, P., Soulsby, C., Waldron, S., and Tetzlaff, D.: Using stable isotope tracers to assess hydrological flow paths, residence times and landscape influences in a nested mesoscale catchment, Hydrol. Earth Syst. Sci., 9, 139–155, doi:10.5194/hess-9-139-2005, 2005.
Rohling, E. J.: Progress in paleosalinity: overview and presentation of a new approach, Paleoceanography, 22, PA3215, doi:10.1029/2007PA001437, 2007.

Salles, P.: Hydrodynamic Controls on Multiple Tidal Inlet Persistence, PhD thesis, Massachusetts Institute of Technology and Woods Hole Oceanographic Institution Joint Program in Oceanography/Applied Ocean Sci. and Engineering, Boston, MA, 2001.

Santos, I. R., Burnett, W. C., Chanton, J., Dimova, N., and Peterson, R. N.: Land or ocean? Assessing the driving forces of submarine groundwater discharge at a coastal site in the Gulf of Mexico, J. Geophys. Res., 114, doi:10.1029/2008JC005038, 2009.

Santos, I. R., Eyre, B. D., and Huettel, M.: The driving forces of porewater and groundwater flow in permeable coastal sediments: a review, Estuar. Coast. Shelf S., 98, 1–15, 2012.

Schubert, M., Paschke, A., Lieberman, E., and Burnett, W. C.: Air–water partitioning of ^{222}Rn and its dependence on water temperature and salinity, Environ. Sci. Technol., 46, 3905–3911, 2012.

Silva, A. V., Portugal, A., and Freitas, L.: Groundwater flow model and salinization of coastal aquifers between Faro and Fuseta, Comun. Ser. Geol. Portugal, 72, 71–87, 1986.

Slomp, C. P. and Van Cappellen, P.: Nutrient inputs to the coastal ocean through submarine groundwater discharge: controls and potential impact, J. Hydrol., 295, 64–86, 2004.

Spiteri, C., Slomp, C. P., Tuncay, K., and Meile, C.: Modeling biogeochemical processes in subterranean estuaries: effect of flow dynamics and redox conditions on submarine groundwater discharge of nutrients, Water Resour. Res., 44, doi:10.1029/2007WR006071, 2008.

Stieglitz, T. C., Cook, P. G., and Burnett, W. C.: Inferring coastal processes from regional-scale mapping of ^{222}radon and salinity: examples from the Great Barrier Reef, Australia, J. Environ. Radioactiv., 101, 544–552, 2010.

Stigter, T. Y. and Monteiro, J. P.: Strategies for integrating alternative groundwater sources into the water supply system of the Algarve, Portugal, Water Asset Management International – IWA 01/2008, 4, 19–24, 2008.

Stigter, T. Y., Carvalho Dill, A. M. M., Ribeiro, L., and Reis, E.: Impact of the shift from groundwater to surface water irrigation on aquifer dynamics and hydrochemistry in a semi-arid region in the south of Portugal, Agr. Water Manage., 85, 121–132, 2006.

Swarzenski, P. W., Orem, W. H., McPherson, B. F., Baskaran, M., and Wan, Y.: Biogeochemical transport in the Loxahatchee River Estuary, Florida: the role of submarine groundwater discharge, Mar. Chem., 101, 248–265, 2006.

Tett, P., Gilpin, L., Svendsen, H., Erlandsson, C. P., Larsson, U., Kratzer, S., Fouilland, E., Janzen, C., Lee, J.-Y., Grenz, C., Newton, A., Ferreira, J. G., Fernandes, T., and Scory, S.:

Eutrophication and some European waters of restricted exchange, Cont. Shelf. Res., 23, 1635–1671, 2003.
Turner, S. M., Malin, G., Nightingale, P. D., and Liss, P. S.: Seasonal variation of dimethyl sulphide in the North Sea and an assessment of fluxes to the atmosphere, Mar. Chem., 54, 245–262, 1996.
Vila-Concejo, A., Ferreira, Ó., Morris, B. D., Matias, A., and Dias, J. M. A.: Lessons from inlet relocation: examples from southern Portugal, Coast. Eng., 51, 967–990, 2004.
Webster, I. T., Hancock, G. J., and Murray, A. S.: Use of radium isotopes to examine pore-water exchange in an estuary, Limnol. Oceanogr., 39, 1917–1927, 1994.
Webster, I. T., Hancock, G. J., and Murray, A. S.: Modelling the effect of salinity on radium desorption from sediments, Geochim. Cosmochim. Acta, 59, 2469–2476, 1995.
Zektser, I. S. and Loaiciga, H. A.: Groundwater fluxes in the global hydrologic cycle: past, present and future, J. Hydrol., 144, 405–427, 1993.

HESSD
12, 12433–12482, 2015

Assessing land–ocean connectivity via SGD in the Ria Formosa Lagoon

C. Rocha et al.

Table 1. Excess ^{222}Rn inventories and relevant fluxes supporting the radon mass balance for the Ria Formosa (see Sects. 4.1 and 5.1).

Inventories	^{222}Rn inventory [Bq m^{-2}]		±MAD [Bq m^{-2}]
Ebb stage[a]	54.2		17.8
Flood stage[a]	74.0		17.6
All data[b]	65.9		19.6
Fluxes	^{222}Rn flux [Bq m^{-2} day^{-1}]		$\pm\sigma$ [Bq m^{-2} day^{-1}]
Diffusion	5.9		1.7
Degassing	1.1		0.7
Decay	11.9		1.6
Residual exchange[c]	-4.74×10^{-4}		7.89×10^{-5}
Tidal flux [d]	^{222}Rn flux [Bq m^{-2} day^{-1}]		$\pm\sigma$ [Bq m^{-2} day^{-1}]
Quatro-Águas			
Export	85.4		11.1
Import	98.6		16.1
Residual	13.2		2.8
Barra-Nova			
Export	49.8		1.1
Import	65.0		4.2
Residual	15.2		1.0
Potential Rn sources	Salinity	Activity [Bq m^{-3}]	$\pm\sigma$ [Bq m^{-3}]
Deserta (Well)	0.95	93.8	59.5
Beach porewater	40.6	304	182
Ramalhete (borehole)	5.06	6625	996

Notes: [a] Calculated with Eqs. (4a) and (4b), Sect. 3.1.4.
[b] Calculated with Eq. (3), Sect. 3.1.4.
[c] Referenced to lagoon surface area at MSL, calculated using the residual exchange measured at Faro-Olhão adjusted to the residual tidal prisms for all the inlets reported in Pacheco et al. (2010) and cross-section area for all the inlets. Minus sign signifies net export (seaward).
[d] Per unit cross-sectional channel area.

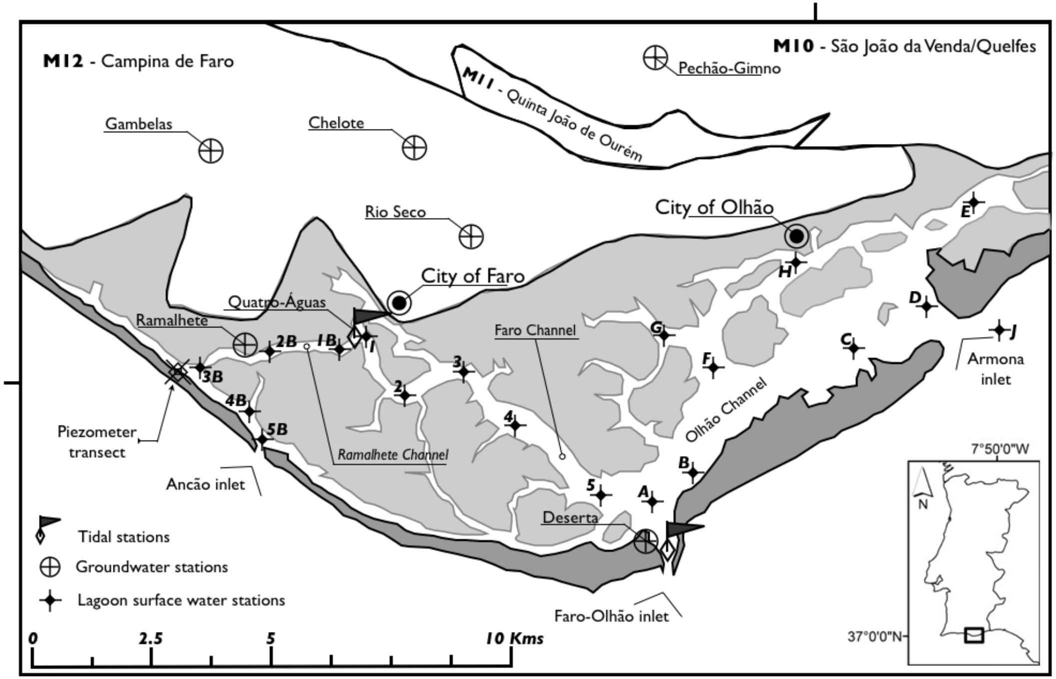

Figure 1. Map showing location of the sampling sites within the Ria Formosa, and boundaries of the aquifers bordering the lagoon (M10, M11, M12).

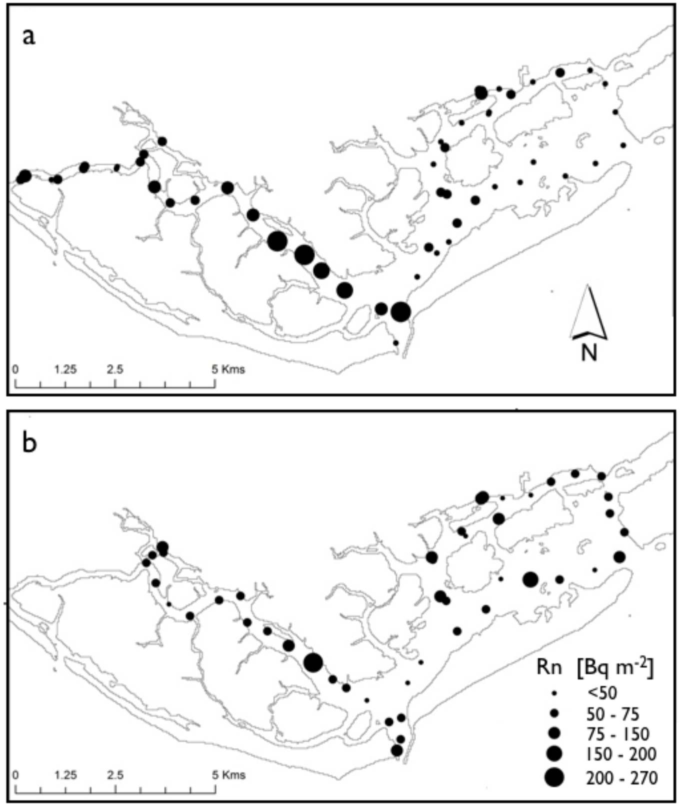

Figure 2. Map showing the distribution of Radon inventories (Bq m^{-2}) within the main channels, during ebb **(a)** and flood **(b)**.

HESSD
12, 12433–12482, 2015

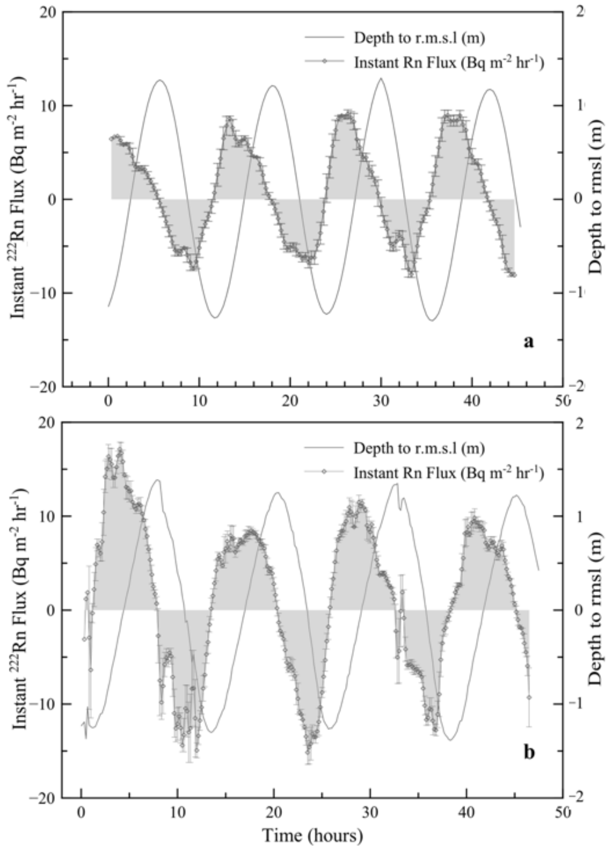

Figure 3. Tidal variability of instantaneous radon fluxes, respectively at the inner at the Barra Nova inlet **(a)** and Quatro-Águas station **(b)**. For more details, please see Sect. 3.1.2.

HESSD
12, 12433–12482, 2015

Assessing land–ocean connectivity via SGD in the Ria Formosa Lagoon

C. Rocha et al.

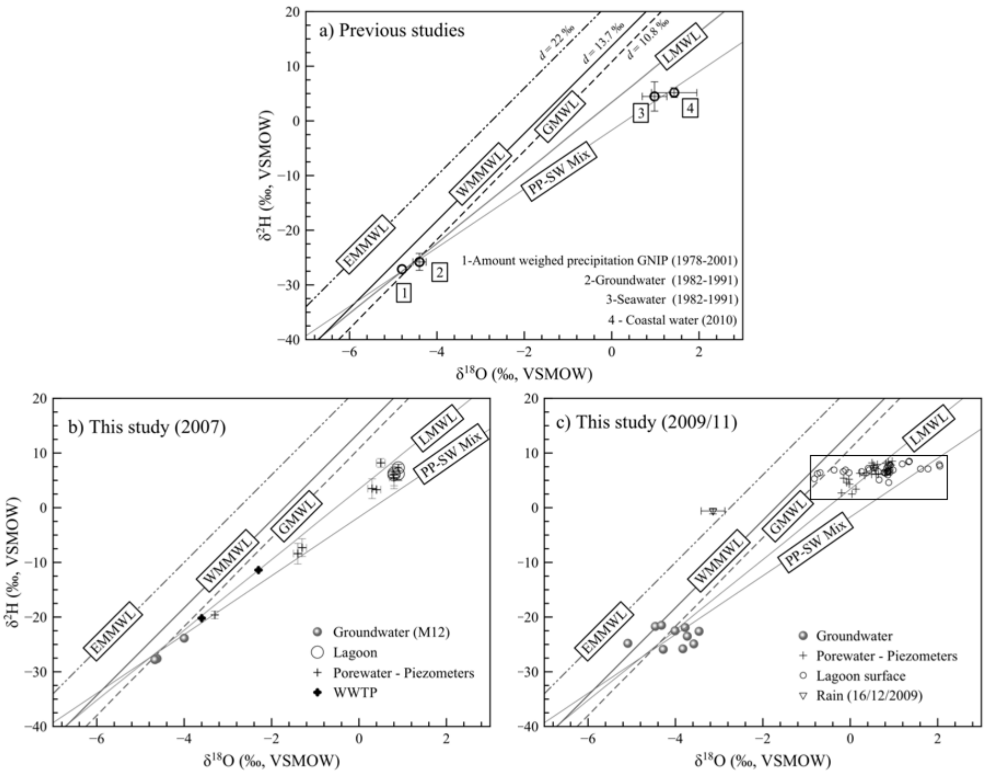

Figure 4. Catchment isotope hydrology. **(a)** shows the main meteoric water lines framing the isotopic composition of precipitation within the catchment, including the precipitation-seawater mixing line. **(b)** plots the isotopic compositional range of water samples taken during 2007, while **(c)** plots the isotopic compositional range of water samples taken during 2009–2011; the lagoon surface water samples (inset) are shown in more detail on Fig. 6.

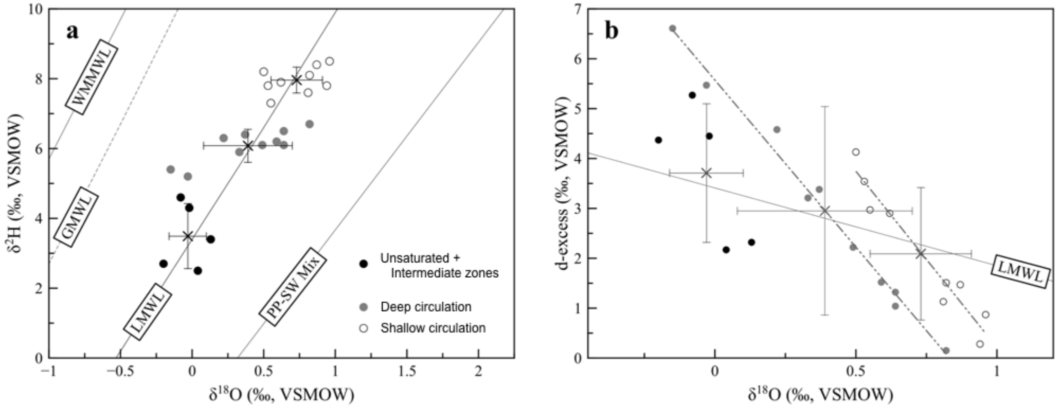

Figure 5. Isotopic composition of pore water extracted in 2009–2010 at different levels depth below the surface at the saturated zone and the dynamics of the beach groundwater table. **(a)** frames the compositional range and the subdivision of the isotopic characteristics through three groups, corresponding to different circulation paths within the beach (for explanation, see Sect. 4.2.3). **(b)** frames the same samples in a *deuterium excess* (d) vs. δ^{18}O plot, illustrating the progression of evaporative enrichment throughout the three zones and its relationship with the LMWL. Crosses and attached error bars represent average compositions for each group. Error bars represent ±1 SD.

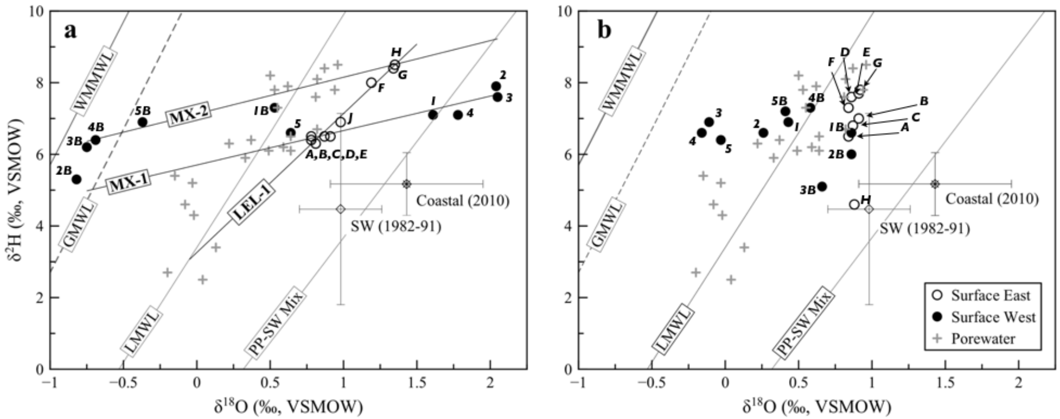

Figure 6. Tidal variability of the isotopic composition of surface waters in the lagoon, framed by significant local evaporation (LEL), mixing (MX), and meteoric lines as well as the average composition of adjacent coastal water and seawater (historic data). **(a)** Low tide, and **(b)** high tide. For more details, see Sects. 4.2.4. and 5.2.

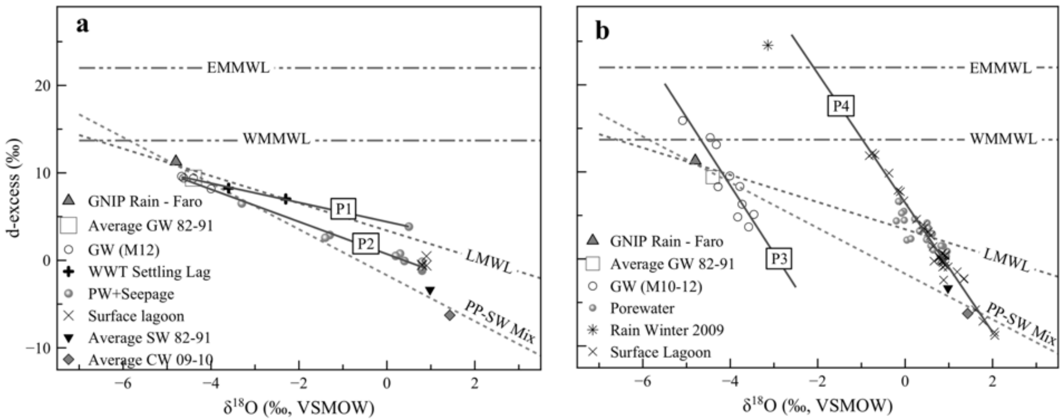

Figure 7. Hydrological pathways within the Ria Formosa, as defined by stable isotope data. **(a)** 2007 situation – SGD with net input of meteoric water present; **(b)** 2009–2011 – SGD essentially derived from tidal pumping. Detailed explanations are available in Sect. 5.3.

HESSD
12, 12433–12482, 2015

Assessing land–ocean connectivity via SGD in the Ria Formosa Lagoon

C. Rocha et al.